AD NUMBER

AD809175

LIMITATION CHANGES

TO:

Approved for public release; distribution is unlimited.

FROM:

Distribution authorized to U.S. Gov't. agencies only; Administrative/Operational Use; JAN 1967. Other requests shall be referred to Office of Naval Research, Arlington, VA 22203.

AUTHORITY

ONR ltr 28 Jul 1977

SU-SEL-67-002

High-Frequency Backscatter from Terrain with Buildings

by

J. R. Barnum

January 1967

Technical Report No. 130

Prepared under
Office of Naval Research Contract
Nonr-225(64), NR 088 019, and
Advanced Research Projects Agency ARPA Order 196-67

RADIOSCIENCE LABORATORY

STANFORD ELECTRONICS LABORATORIES

STANFORD UNIVERSITY · STANFORD, CALIFORNIA

DISCLAIMER NOTICE

THIS DOCUMENT IS THE BEST QUALITY AVAILABLE.

COPY FURNISHED CONTAINED A SIGNIFICANT NUMBER OF PAGES WHICH DO NOT REPRODUCE LEGIBLY.

HIGH-FREQUENCY BACKSCATTER FROM TERRAIN WITH BUILDINGS

by

J. R. Barnum

January 1967

Technical Report No. 130

Prepared under
Office of Naval Research Contract
Nonr-225(64), NR 088 019, and
Advanced Research Projects Agency ARPA Order 196-67

Radioscience Laboratory
Stanford Electronics Laboratories
Stanford University Stanford, California

ABSTRACT

It is becoming more apparent that a fair proportion of high-frequency backscatter from level portions of the earth's surface results from upright targets such as trees and buildings. Using the standing-wave method, at 26 MHz, trees have been investigated at angles of incidence (with respect to the horizontal) up to 22.5°. It was found that a tree may provide significant scatter.

The present undertaking was to measure--by the same technique--backscatter from cement walls of different sizes and conditions at 26 MHz. Using a balloon-borne transmitting antenna and telemetering probe, cross sections for both horizontal and vertical polarization were obtained for angles of incidence between 2.5° and 22.5°. Magnitudes of cross sections were much greater for vertical polarization at lower angles of incidence.

For angles of incidence other than broadside, but with the radiation perpendicular to the intersection of the wall and the ground, the wall-ground combination behaved as a corner reflector; the experimental results for larger walls showed agreement with the corresponding theory. Subsequent extrapolation of the theory suggests that buildings may have cross sections much higher than trees.

A comparison of wall scatter to that from a large oak tree, and consideration of other city targets, suggests that at low angles of incidence horizontally polarized scatter should be larger from cities than from forests, primarily at the upper end of the HF spectrum. Although an average building may have a cross section as much as 16 db larger than that for an average tree, trees far outnumber buildings in the large areas illuminated by HF radar; therefore, trees may be the primary source of vertically polarized ground backscatter. A knee was observed in the curves for cross section vs angle of incidence; however, the knee was not as pronounced for the wall as that occurring for a large oak tree. This variance suggests that scatter from buildings may be higher than that from trees at the lower angles of incidence.

Backscatter signal enhancements from cities at particular frequencies might provide an indication of the magnitude of building scatter from a particular target area.

CONTENTS

TABLES

ILLUSTRATIONS

SYMBOLS

a	an arbitrary wall dimension
a_ℓ	$(f_\ell - f_o)Q_i/f_o$
a_u	$(f_u - f_o)Q_i/f_o$
A	$2A_o \cos \Psi$
A_o	physical area of one wall face
A'	a constant used to determine E_i for horizontal polarization
B	B/I_L = the relative free-space cross section
c	speed of light in free space
C	capacitance of plates, $\epsilon_r C_o$
C_o	capacitance of plates in free space
C_{Qm}	capacitance added by Q meter when plates are connected
C_T	total parallel capacitance in circuit
d	thickness of a wall
D	shortest distance between building rows
E_i	field strength of the incident radiation at the target position in the absence of the target
E_{Po}	field strength at the position of the peak in the background in the absence of the ground
E_s^r	field strength of the backscattered radiation at a distance r from the target
f_ℓ	lower 3-db cutoff frequency in Q measurements
f_u	upper 3-db cutoff frequency in Q measurements
f_o	center frequency in Q measurements
F_V	a factor used in determining E_i for vertical polarization
F_H	a factor used in determining E_i for horizontal polarization
G	gain of transmitting/receiving antenna

h	full height of wall
h_L	height of scattering power/telephone line
h_p	height of probe
h_s	height of a narrow horizontal target scattering segment
I_h	horizontal illumination factor
I_L	vertical illumination factor
k	propagation constant in free space, $2\pi/\lambda$
k_w	propagation constant of the wall
L	inductance of work coil used in capacitor-Q technique
P	represents error in measured E_s due to nonconstant phase-range dependence
P_r	receiver power from backscatter
P_T	transmitted power
Q	Q of capacitor measured with wall material dielectric
Q_i	indicated Q
Q_a	actual Q
r	distance between base of target and probe
r_g	ground-reflected distance to the probe from a horizontal target segment
r_o	range from target at which extrapolation was performed to determine E_s^{100}, usually 60 ft
r_t	direct distance to probe from a horizontal target segment
R	distance between the transmitter and the probe, $R_o - r$
R_o	distance between the transmitter and the target
R_N	distance between the transmitter and the position of the null in the background
R_P	distance between the transmitter and the position of the peak in the background
R_g	reflection coefficient of the ground

R_{gH}	reflection coefficient of the ground for horizontal polarization
R_{gV}	reflection coefficient of the ground for vertical polarization
R_w	reflection coefficient of the wall
R_{wd}	reflection coefficient of the dry wall
R_{ww}	reflection coefficient of the wet wall
R_s	resistance which represents a lossy dielectric
S	factor to relate the relative to the actual free-space cross section
T_1, T_2	represent transfer functions used in capacitor-Q technique
V	transmitter voltage that creates null in probe telemeter output; 1/V is relative field strength
V_c	voltage across capacitor measured in capacitor-Q technique
V_g	voltage of RF generator in Q meter
V_ℓ	V_c at f_ℓ
V_u	V_c at f_u
$V_{\ell o}$	normalized V_ℓ for parallel resonant circuit
V_{uo}	normalized V_u for parallel resonant circuit
w	horizontal distance to target, r cos Ψ
β	angle between incident rays and rows of buildings
δ	path difference between two rays
δ_N	path difference between ground-reflected and direct rays at a null in the background field variation
δ_p	path difference between ground-reflected and direct rays at a peak in the background field variation
ϵ_r	relative dielectric constant
ϵ_{rc_g}	complex relative dielectric constant for the ground
ϵ_{rc_w}	complex relative dielectric constant for a wall

η	$(2\pi h \sin \psi)/\lambda$
λ	wavelength of radiation studied, 38 ft
ω	radian frequency, $2\pi f$
ω_o	$2\pi f_o$
ψ	angle of incidence of incoming radiation, measured to the ground
σ	conductivity
$\sigma_B(\psi)$	radar cross section as a function of angle of incidence
σ_{Bo}	theoretical free-space radar cross section

ACKNOWLEDGMENT

Acknowledgment is made of the many useful ideas contributed by the Rev. J. G. Steele and Dr. L. Wetzel of the Institute for Defense Analyses, Arlington, Va. Thanks are due C. R. Gilliland and E. Clouse, who assisted in the collection of data; F. Dameron and Miss M. K. Mandt, who assisted in the reduction of data; and D. E. Westover, who wrote the computer program for the wall scattering theory. In addition, thanks are due Reverend Steele and Dr. G. H. Barry, who painstakingly criticized the work; and Dr. O. G. Villard, Jr. under whose direction the work was performed.

I. INTRODUCTION

At present, much information about the ionosphere is gained through high-frequency backscatter soundings. It is also hoped to utilize backscatter sounding in identifying different types of terrain. However, in order to obtain reasonably accurate quantitative results, the total backscattered power from the illuminated area must be known. This may be obtained through a knowledge of the radar cross-sectional area of the target. Backscatter properties of the ground have been the subject of many investigations. Backscatter coefficients for different terrains and angles of incidence were measured by Hagn at 32.8 MHz [Ref. 1]. Steele [Refs. 2,3] obtained results for more general types of terrain using a 16-MHz backscatter sounder and assuming smooth ionospheric conditions.

It was suggested by Steele [Refs. 2,3] that the backscatter from land is primarily associated with upright targets (such as trees and buildings), and only secondarily with ground contour roughness. To investigate this, Steele and Barnum [Ref. 4] developed a method for deducing free-space radar cross sections of land objects using the standing-wave method [Ref. 5]. At 26 MHz it was found that a tree behaves like a resonant target--for both horizontal and vertical polarization--and is capable of producing significant backscatter. In that investigation, metal street-lighting masts had the largest cross section of the various targets measured.

Backscatter from a ground target includes the ground as part of the target, and cross sections are therefore a function of angle of incidence. Using the same technique of field measurement as Steele and Barnum [Ref. 4], Steele [Ref. 6] developed a method for measuring the cross section of a tree at different angles of incidence. It was found that a tree behaves like a conducting dipole for both horizontal and vertical polarization. Below 20° scatter was generally stronger for vertical polarization than for horizontal, and at 10° a pronounced knee effect was observed for vertical polarization.

If cities provide significant scatter compared to forests, they might be identifiable in sweep-frequency radar backscatter. In this connection, the radar cross section of buildings would be of great interest. As with most targets, city and forest cross sections should be some function of frequency, and the particular function will affect this identification.

The present undertaking was to measure the backscatter from various sizes and conditions of cement block walls, and from these measurements deduce their radar cross sections as a function of angle of incidence and wall size. Steele's method [Ref. 6] was employed at 25.9 MHz over angles of incidence ranging from 2.5° to 22.5°. Wall sizes ranged from 5 ft high and 10 ft wide to 20 ft high and 20 ft wide. Some walls were measured both wet and dry. One wall was also covered with chicken wire, another contained vertical metal rods embedded in the wall, which simulated support used in actual construction. Most of these results have been predicted by Wetzel [Ref. 7], and measurement of the electrical constants of the wall enabled his theory to be calculated and compared with experimental results.

It was possible to predict relative magnitudes of building and tree cross sections. Knowledge of these cross sections, together with those for other city targets, enabled approximate comparisons to be made between forest and city scatter for both polarizations.

II. THEORY

Assuming free-space propagation (no ionosphere), the radar cross section is defined by its radar equation,

$$P_r = \frac{P_T G^2 \lambda^2}{(4\pi)^3 R_o^4} \sigma_B \tag{1}$$

where P_r = received power
P_T = transmitted power
R_o = distance to the scatterer
G = gain of the transmitting/receiving antenna
λ = wavelength

From this we deduce that

$$\sigma_B \triangleq 4\pi R_o^2 \left| \frac{E_s^{R_o}}{E_i} \right|^2 \tag{2}$$

where $E_s^{R_o}$ is the field strength of the backscattered radiation as measured at the transmitter, and E_i is the field strength of the incident radiation at the target.

If we measure E_s at some particular distance r from the target, other than R_o, the range dependence of E_s must be known in order to establish the value of E_s at R_o, where its effect is ultimately realized in radar calculations. For all the targets used (as well as all those preceding [Refs. 4,6]), the target was well outside the first Fresnel zone of the transmitter. Hence the illumination of the target was of essentially uniform phase over its broadside dimensions. Also the range dependence of E_s may be expected to vary as $1/r$, provided we are far enough away from the target. Therefore, regardless of the nature of the target, or its relation with the ground, all that is needed is a measure of E_s^r/E_i^o at some distance r far enough from the target so that E_s varies as $1/r$. For lower heights of targets, a suitable value of r will be smaller than for high targets, since for lower targets the ground-reflected and direct

rays reradiated from the target will assume steady-state interference closer to the target. As will be seen in Chapter IV, r = 60 ft was a suitable distance in most cases.

Wetzel has derived theoretical results for a plane reflector mounted vertically on the ground and facing the incident radiation [Ref. 7]. As he suggests, the target is a corner reflector and reradiation has range dependence 1/r. His results are given by

$$\sigma_B(\psi) = \sigma_{Bo} |F(\psi)|^2 \tag{3}$$

where

$$\sigma_{Bo} = \frac{4\pi A_o^2}{\lambda^2} R_w^2\left(\frac{\pi}{2}\right)$$

and

$$|F(\psi)|^2 = \cos^2 \psi \frac{R_w^2\left(\frac{\pi}{2} - \psi\right)}{R_w^2\left(\frac{\pi}{2}\right)} \left[\left[\text{sinc } (\eta)\left(1 + e^{i2\eta} R_g^2(\psi)\right) + 2e^{i\eta} R_g(\psi)\right]\right]^2$$

where $\sigma_B(\psi)$ is the radar cross section as a function of the angle of incidence ψ; σ_{Bo} is the free-space cross section of a flat plate in free space, with normally incident radiation, with A_o its physical area; $\eta = (2\pi h \sin \psi)/\lambda$, where h is the height of the wall; R_w and R_g are the reflection coefficients of the wall and ground, respectively, as a function of grazing angle (angle of incidence) ψ. We note that for large η this reduces to

$$\sigma_B(\psi) = 4\sigma_{Bo} \cos^2 \psi R_w^2\left(\frac{\pi}{2} - \psi\right) \left|R_g(\psi)\right|^2 \tag{4}$$

Then,

$$\sigma_B = \frac{4\pi A^2}{\lambda^2} R_w^2\left(\frac{\pi}{2} - \psi\right) \left|R_g(\psi)\right|^2 \tag{5}$$

where $A = 2A_o \cos \psi$; this is in agreement with Kerr [Ref. 8, p. 457] when it is remembered that a corner reflector is equivalent to a flat plate of area $2A_o \cos \psi$. R_w represents the magnitude of the wall reflection

coefficient which is found from the theory of thin (lossy) dielectric slabs [Ref. 9] as

$$R_w\left(\frac{\pi}{2}\right) = \left|\left(1 - \frac{k_w d}{2}\right)\left(\frac{1}{\sqrt{\epsilon_{rc_w}}} - \sqrt{\epsilon_{rc_w}}\right)\right| \tag{6}$$

where k_w is the propagation constant of the wall, d is the thickness of the wall, and ϵ_{rc_w} is the complex relative dielectric constant of the wall. But since $k_w = \frac{\omega}{c}\sqrt{\epsilon_{rc_w}}$, we have

$$R_w\left(\frac{\pi}{2}\right) = \left|\frac{\omega}{2c}\left(1 - \epsilon_{rc_w}\right)d\right| = 0.0551\left|1 - \epsilon_{rc_w}\right|$$

where $\omega = 2\pi(25.9 \times 10^6)$, $c = 3 \times 10^8$, and $d = 0.203$ m.

Using ϵ_{rc_w} as derived in Chapter V, R_w is calculated for $\psi = 0$. As Wetzel suggests, R_w will not change appreciably for angles of incidence in the range $0° \leq \psi \leq 30°$. $R_g(\psi)$ may be assumed to be -1 for horizontal polarization. For vertical polarization, the ground constants must be known. For this terrain Steele [Ref. 6] estimated that $\epsilon_r = 15$, a typical value. Reference to typical conductivities [Ref. 10, p. 808] enables us to assume that $\sigma \approx 7 \times 10^{-3}$ mho/m for the particular terrain under study. This gives $\epsilon_{rc_g} = 15 - 14.86$, where ϵ_{rc_g} is the relative complex dielectric constant for the ground. Thence, for vertical polarization, we can calculate R_g as follows [Ref. 8, p. 396; Ref. 11]:

$$R_g(\psi) = \frac{\epsilon_{rc_g}\sin\psi - \left(\epsilon_{rc_g} - \cos^2\psi\right)^{\frac{1}{2}}}{\epsilon_{rc_g}\sin\psi + \left(\epsilon_{rc_g} - \cos^2\psi\right)^{\frac{1}{2}}} \tag{7}$$

Enough information was therefore obtained to plot a set of theoretical curves for most of the various sizes and conditions of walls measured.

III. MEASUREMENT TECHNIQUE

The standing-wave method for deducing a radar cross section has been adapted to 25.9 MHz as described by Steele and Barnum [Ref. 4]. For measuring cross sections at different angles of incidence, the method was further adapted as described by Steele [Ref. 6]. Here, the same frequency was used, and the system was unchanged except for the nature of the target. A schematic diagram of the measurement site is shown in Fig. 1.

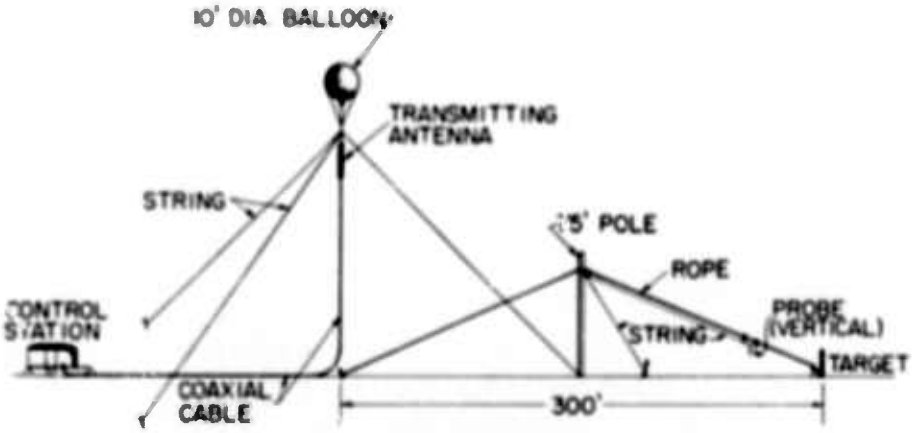

FIG. 1. EXPERIMENTAL SETUP FOR MEASUREMENT OF CROSS SECTIONS AT DIFFERENT ANGLES OF INCIDENCE.

The targets were 8-in.-thick cement block walls. Sizes, in feet, were: 5 high by 10 wide; 10 by 10; 10 by 20; 15 by 20; and 20 by 20. The last three walls were measured both wet and dry. In addition, the 10- by 10-ft wall was covered with chicken wire, and the 10- by 20-ft wall contained vertical metal rods spaced every 6.5 ft to simulate support used in actual construction. Otherwise, the walls were supported only by a wooden frame; the backscatter from the frame, even when wet, was assumed negligible.

Figure 2 shows the wetting process. The wall was covered with water on both sides to insure thorough dampness. It was assumed that the degree of water permeation in the wall would correspond, in radar backscatter cases, to a cement building in a rainy area subjected to continuous downpour, thereby equalizing total dampness for the two cases.

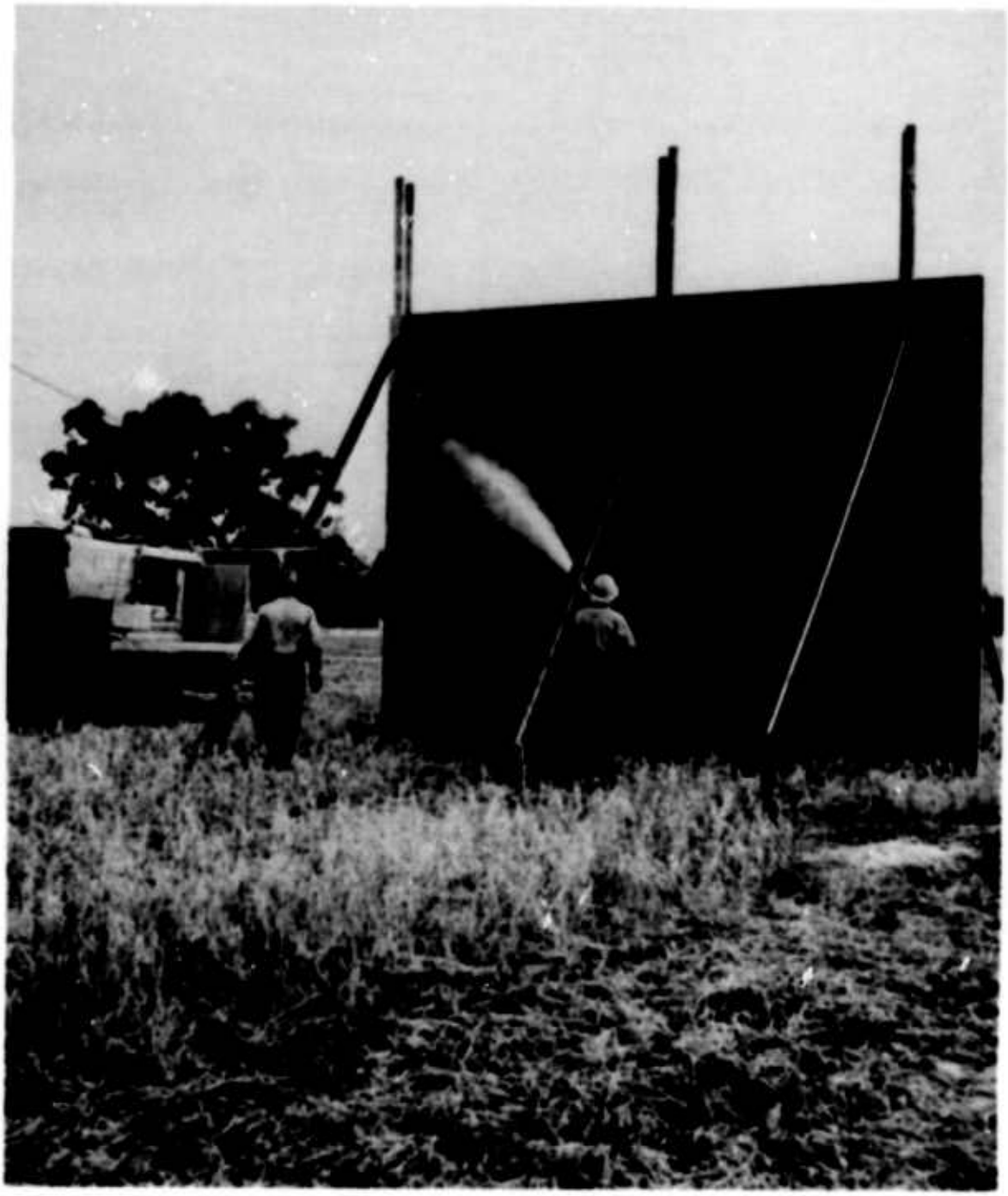

FIG. 2. WALL WETTING PROCESS.

Through the use of a transit, the probe line and a line normal to the wall were positioned to within 1° horizontal separation. The probe line met the wall at the middle of its base. Since the probe hung 3 ft under its supporting rope, the rope was elevated an experimentally adjusted amount, thereby adjusting the actual probe line to the correct path. A typical setup is shown in Fig. 3.

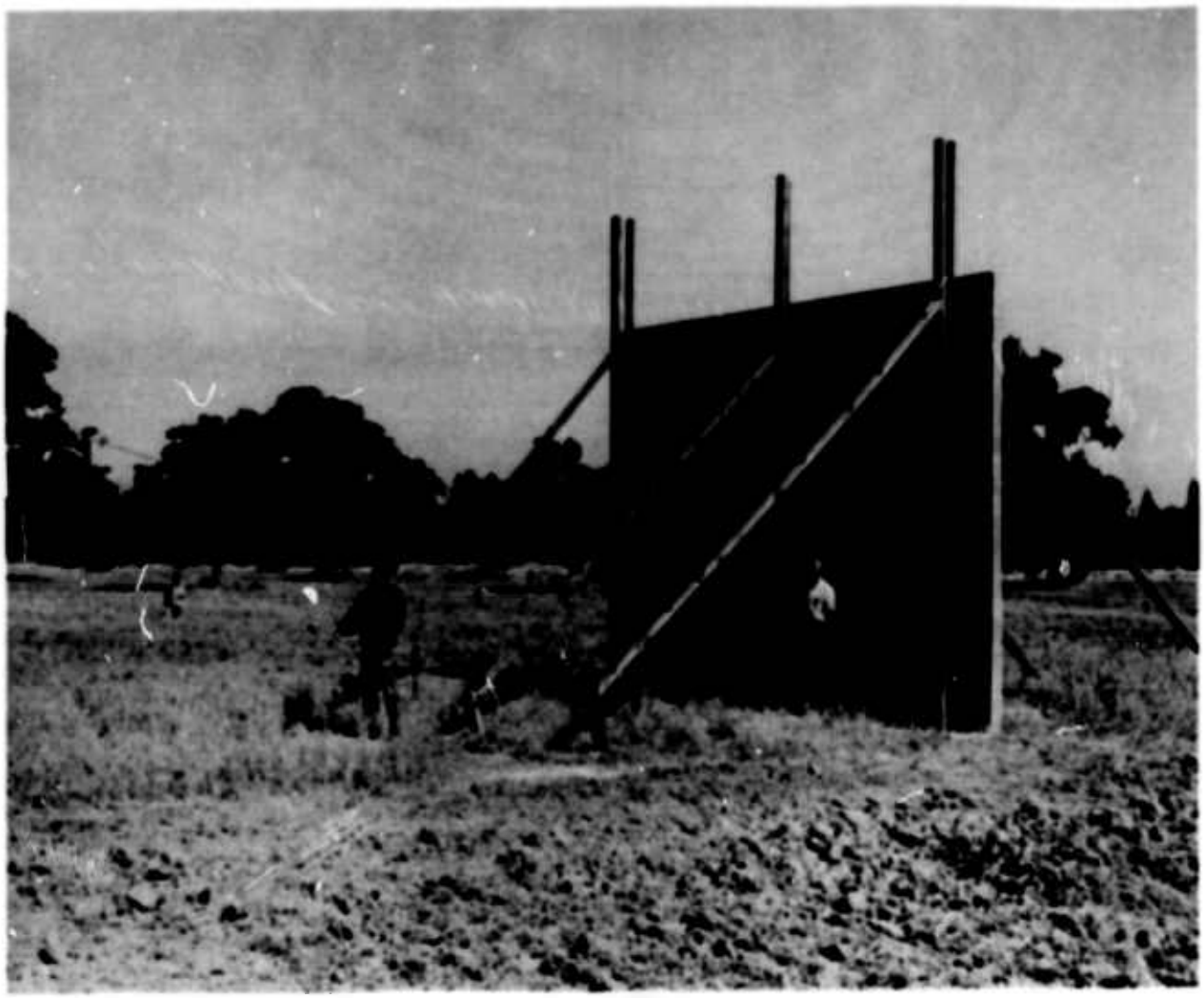

FIG. 3. TYPICAL TARGET SETUP: 15-FT-HIGH BY 20-FT-WIDE WALL.

Measurements were taken using both horizontal and vertical polarization. As will be seen and discussed later, cross sections were very small for horizontal polarization, except for the 20- by 20-ft (largest) wall.

The balloon-borne transmitting antenna could be maneuvered to a height of 150 ft. Since the target was 300 ft away, along the ground, angles of incidence ranging between 2.5° to 22.5° were achieved. The telemetering probe was moved along a rope by means of pulleys and strings; its position was recorded with the aid of a plumb bob. The transmitter output was varied to achieve a standard electric field at the probe for each position the probe occupied. When this was accomplished, the gate-controlled telemetering transmitter showed a 17-db null. A plot of inverse transmitter output voltage vs r, the radial distance to the transmitter antenna, gave a relative indication of the electric field variations in front of the target which would exist if some constant transmitter output were maintained. These plots will be discussed in the next chapter.

The following items were noted by Steele [Ref. 6]: The dry 75-ft wooden pole, suspending the probe line rope, would introduce only a slight constant attenuation to the transmitted signal. Any day-to-day variation of system efficiency was of little consequence, since only ratios of relative field strengths were desired. For example, if the transmitting antenna is raised to produce a different angle of incidence, the obliquity affects both incident and scattered fields although their ratio is unaffected. Likewise, any inclination of the probe (which never exceeded a few degrees from vertical or horizontal) affected E_s and E_i equally. Other targets in the vicinity of the experiment (including the tree which was found to have appreciable scatter) were far enough away from the probe so that the added field term along the probe line would produce only some negligible slow variation in the total field pattern. There are, of course, some factors which would cause error; these are discussed in Chapter IV.

IV. DATA REDUCTION AND ANTICIPATED ERROR

The plots of $1/V$ vs r were handled in a fashion similar to those done by Steele [Ref. 6] except that a different method was used to obtain the incident field at the target, E_i. This is discussed in detail below.

The usual plots of $1/V$ vs w were first obtained. V is the transmitter voltage and w is the horizontal distance between the transmitter and the probe. Since the targets were not removable, as was the case for the tree [Ref. 6], a background field was sketched in; this is the field that would exist if the target were removed. This curve was assumed to be smooth, but not monotonic near the target and in some cases for large w, since ground reflections modify the field pattern. The latter was found to be true for typical cases in Steele's work. E_s at the peaks and nulls in the standing wave was deduced graphically and plotted on a log-log plot vs r, the radial (direct) distance between the probe and the target. Reference to these plots shows that a line of slope -1 could be fitted to the data, with some points falling above and some below the line. As Steele points out, the assumption of the particular background field variation may be in error; however, this method of finding E_s tends to minimize this error providing that it is random. E_s^{100} is found by extrapolating the line of -1 slope to $r = 100$ ft (30.48 m). As seen in Chapter II, since E_s varies as $1/r$,

$$\sigma_B = 4\pi(30.48)^2 \left| \frac{E_s^{100}}{E_i} \right|^2 \quad m^2 \tag{8}$$

Since many sets of data were taken, a quicker method for determining E_i was desired. Basically this involved determining a factor called F, for both horizontal and vertical polarization, which, when multiplied by $1/V$ ($w = 60$ ft), gave E_i for a particular set of data. F is then a function of angle of incidence and is quite different for the two polarizations as seen in Fig. 4. This variance arises due to the widely differing reflection coefficients for the ground vs angle of incidence, $R_{gH}(\psi)$ and $R_{gV}(\psi)$, for horizontal and vertical polarization, respectively. The underlying assumption is that $R_{gH}(\psi)$ and $R_{gV}(\psi)$ did not change from

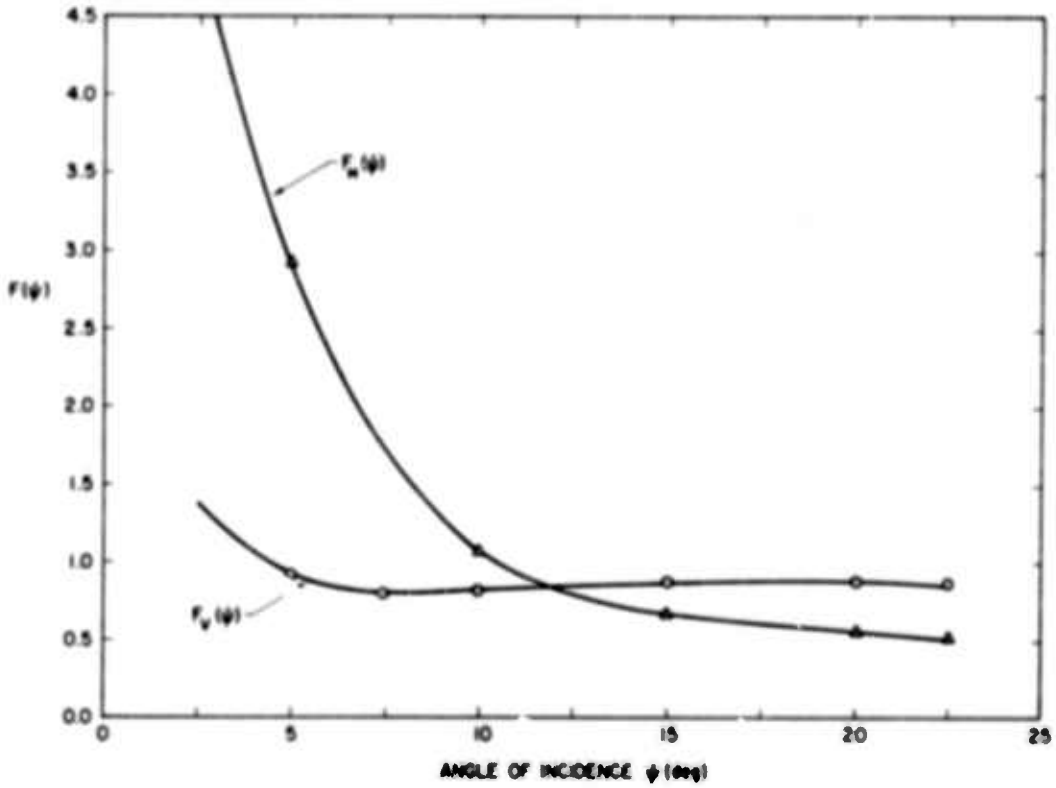

FIG. 4. F FACTORS FOR CALCULATING E_i.

week to week. As will be seen, this assumption is probably valid since it was found that reflection coefficients were lower than expected, indicating probable subsurface reflection and subsequent attenuation on the ground reflected rays. Furthermore, the moisture content of the soil beneath the surface would seem fairly constant due to the presence of a water table and frequent enough rain.

For horizontal polarization, F_H was obtained as follows.

Over a period of 2 days, sets of data were taken for all the angles of incidence in question. "Standard readings" were also taken on each of these days by recording $1/V$ at a particular angle of incidence and probe position. These readings were found identical, and therefore the system efficiency was assumed constant for these sets of data. Next, it was observed that the data for 22.5° contained both a "peak" and a "null" in the background field variation (which is similar to Steele's example [Ref. 6, p. 15]). Since the peak is caused by constructive interference and the null is caused by destructive interference between the direct and ground-

reflected rays, a relation may be derived for the total incident field representation at the peak in terms of the field which would exist there in the absence of the ground. The occurrence of the null and its position, together with an assumption of constant R_{gH}, enabled this calculation. All individual rays are assumed to vary as $1/R$ (where R is measured from the transmitting antenna), since far field conditions prevail. Hence, at peak,

$$\frac{1}{V_p} = A' E_{po} \tag{9}$$

where $1/V_p$ is the field at the peak, A' is a constant which is assumed to be always 2.0 in Steele's work for horizontal polarization [Ref. 6], and E_{po} is the field which would exist at the peak position in the absence of the ground. A' is given by

$$A' = \frac{2 + \left(\frac{\delta_N}{R_N} + \frac{\delta_P}{R_P}\right)}{1 + \frac{V_P R_N}{V_N R_P}\left(1 + \frac{\delta_N}{R_N}\right) + \frac{\delta_P}{R_P}} \tag{10}$$

where R_N and R_p are the distances between transmitting antenna and probe at the null and peak, respectively; $1/V_N$ is the total field at the null; δ_N and δ_p are the path differences between direct and ground-reflected rays at the null and peak, respectively. For an angle of incidence of 22.5°, the appropriate set of above data gave $A' = 1.482$ (which differs from Steele's assumed value of 2.0). It was interesting to find that $|R_{gH}|$ (which was assumed constant) was found to be 0.62, where

$$|R_{gH}| = (A' - 1)\left(1 + \frac{\delta_P}{R_P}\right)$$

and had a phase lag of 161°

$$\text{Phase lag of } R_{gH} = \frac{\delta_p - \lambda}{\lambda} \times 360° \tag{11}$$

and $\lambda = 38$ ft for this experiment. Table 1 shows the various numbers determined for finding A'. Next, E_1 was obtained as

$$E_1(22.5°) = \frac{1}{A'V_p} \times \frac{R_p}{R_o} \tag{12}$$

where $R_o = 325$ ft for $\psi = 22.5°$. Finally, the desired F was obtained from

$$F_H(22.5°) = \frac{E_1(22.5°)}{\frac{1}{V}(w = 60 \text{ ft})} \tag{13}$$

TABLE 1. DATA FOR DETERMINING A'

Total field at null	$1/V_N = 0.0589$ (volt)$^{-1}$
Total field at peak	$1/V_p = 0.2185$ (volt)$^{-1}$
Distance between transmitter and peak position	$R_p = 192$ ft
Distance between transmitter and null position	$R_N = 225$ ft
Path difference between direct and ground-reflected rays from the transmitter at the null position	$\delta_N = 38$ ft
Path difference between direct and ground-reflected rays from the transmitter at the peak position	$\delta_p = 55$ ft

Since the system efficiency and the vertical patterns of the probe and transmitting antenna were constant for the other angles of incidence, we have

$$E_1(\psi) = E_1(22.5°) \times \frac{\cos \psi}{\cos 22.5°} \tag{14}$$

which takes into account different R_o for different angles of incidence. Hence,

$$F_H(\psi) = \frac{E_i(\psi)}{\frac{1}{V}(w = 60 \text{ ft})} \tag{15}$$

and this is plotted in Fig. 4. This is considered a more accurate method for determining E_i than that used by Steele [Ref. 6].

For vertical polarization, a different method was used to determine E_i and F_V. Since the gain of the probe was different for direct and ground-reflected rays, the above formulas could not be applied. Furthermore, the reflection coefficient of the ground for vertical polarization, R_{gV}, is a function of angle of incidence. Steele [Ref. 6] took advantage of this fact when determining the E_i's for vertical polarization. Since exactly the same location and experimental apparatus were used for this experiment, reference was made to the E_i values, and corresponding $1/V$ $(w = 60 \text{ ft})$ which Steele obtained for each angle of incidence when measuring dipoles at the same target position as the wall. The data employed were similar to those shown by Steele [Ref. 6, p. 19]. As before,

$$F_V(\psi) \triangleq \frac{E_i(\psi)}{\frac{1}{V}(w = 60 \text{ ft})} \tag{16}$$

F_V for vertical polarization is also plotted in Fig. 4.

Using the same method, F_V was found for another set of data taken about the same time, and close correspondence was found. However, a time lapse of several weeks occurred between those sets and the sets taken for the walls. As a result, the wall data experienced gain drift due to much larger ambient temperature variations between 6:30 a.m. and 10:00 a.m. Therefore, it was not possible to assume a constant standard reading over a day (as was verified) and hence the F_V's could not be checked with the later data. It should be noted, however, that since each set of data was taken in approximately 15 minutes, any temperature drift occurring during this time was negligible. Most of the time was spent in reorganizing the experiment for each angle of incidence; hence, during these times, overall temperature changes were greatest.

From the plots of $F(\psi)$, $E_i(\psi)$ was obtained for each set of data. Hence, from the values for E_s^{100}, cross sections were obtained as mentioned.

Before the results are discussed, it would be appropriate to investigate factors contributing to experimental inaccuracy. For the experimental setup used, there are four causes of error: meter scale inaccuracy and misplacement or misalignment of the probe; errors in determining E_i using the above F factors; the probe line not following the correct path; and obliquity effects caused by taking readings too close to the target. These will be discussed in the same order below.

The first source of error was explored by Steele and Barnum [Ref. 4]. It was found that an error of ±0.05 db in total measured field values would be an expected maximum. An illustration of this may be seen in Fig. 5 where

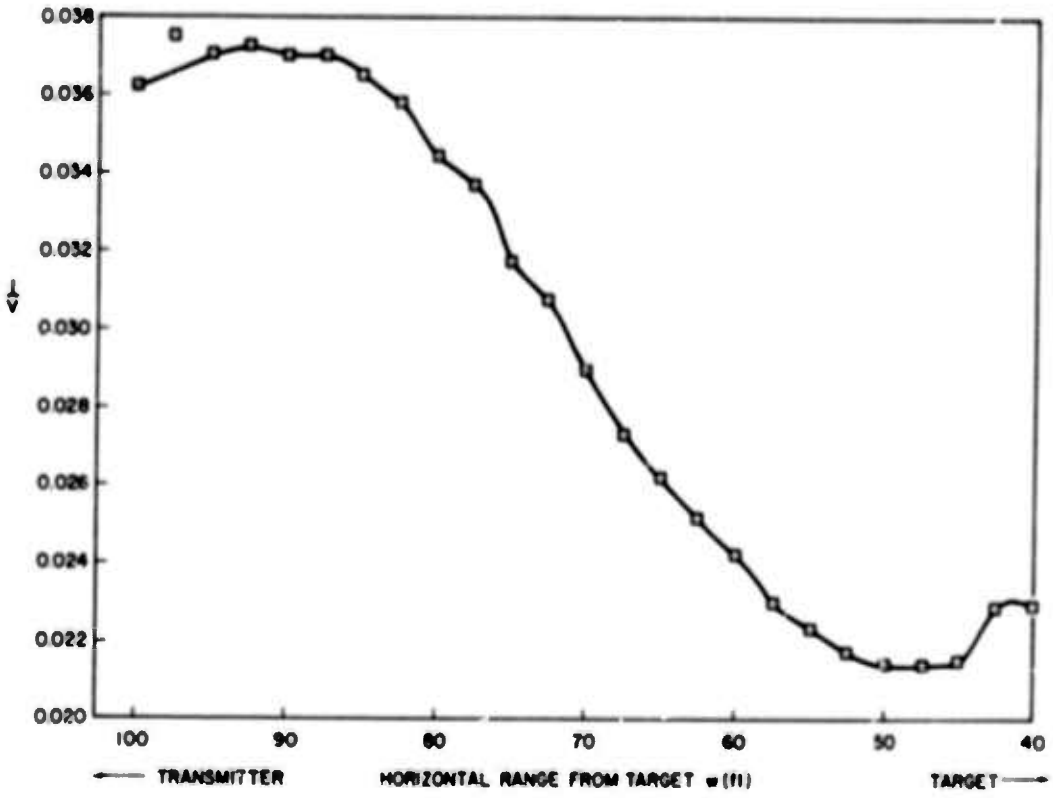

FIG. 5. TYPICAL "BACKGROUND" FIELD VARIATION.

a typical "background" field is plotted. By inserting this error into the cross-section formula, one finds that the error in cross section is given by

$$\Delta\sigma_B \cong \pm \frac{r_o}{100}\sqrt{\sigma_B} \quad m^2 \tag{17}$$

where r_o is the distance in feet from the target at which E_s^r is measured. Since r_o was about 60 ft, the maximum expected percentage error is about $\pm 60/\sqrt{\sigma_B}$ percent. However, since these errors occurred randomly, they were readily apparent, and the standing-wave curves were smoothed over accordingly. Furthermore, the graphical method used to determine E_s^{100} tends to minimize this error. Hence an error in cross section of perhaps $\pm 15/\sqrt{\sigma_B}$ percent might be expected. The error is a function of the measured cross section since for small cross sections the errors may have amplitudes as great as the standing wave. Likewise, for large cross sections, errors are negligible compared to standing-wave magnitudes at r_o = 60 ft. This essentially accounts for errors in determining E_s^{100}.

For horizontal polarization, the computed E_i's, using F_H, are much more accurate than found previously [Ref. 6], especially for the larger angles of elevation. Perhaps ±5-percent error exists in determining E_i for horizontal and vertical polarization using the F factors.

The probe line may have been ±1° off the correct angle-of-incidence path. Reference to Wetzel's formulas in Chapter II suggests that an error in cross section of perhaps ±1 percent would result.

If measurements are taken too close to the target, a negative error will occur for both polarizations due to horizontal obliquity. For a 20-ft-wide wall, at r_o = 60 ft, the reflected waves from the vertical edges of the wall lag those from the center by 8.5°. The effect is identical to obliquity errors occurring in free-space cross-section measurement [Ref. 4, p. 5]; Steele and Barnum deduced that cross sections of large targets would be perhaps 10 percent too low. Since the walls are smaller than the targets which they measured, perhaps an error of -5 percent exists due to horizontal obliquity; the error is slightly greater for horizontal polarization due to the probe's gain pattern.

Also at close ranges, there will be an error caused by the scattered field's nonconstant phase variation with range. In other words, when far enough from the target, the scattered field drops off as $1/r$, and the phase difference between direct and ground-reflected rays reradiated from

the target is a constant. The effect at close ranges r_o will be different for horizontal and vertical polarization due to the different respective ground reflection coefficients.

The analysis is fairly straightforward for horizontal polarization. Suppose that a certain (small) error may be tolerated; the required distance from the target becomes smaller as the target height and ground-reflection coefficient decrease and the angle of incidence increases. In order to obtain a maximum limit for this error, it was assumed that the ground-reflection coefficient was always -1 and that the target scattered in equal magnitudes toward the probe and the ground. The results are directly applicable to a horizontal segment of the target, with small vertical extent, located a height h_s off the ground. The law of cosines was applied to determine the resultant scattered field. Define P as the ratio of actual scattered field to the value which would exist if the phase were constant with distance (Fig. 6). Then P is given by [Ref. 10, p. 811]

$$P = \frac{E_s^{r_o} \times r_o}{\lim_{r_o \to \infty} E_s^{r_o} \times r_o} = \left(\frac{r_o^2 \left(\frac{1}{r_t^2} + \frac{1}{r_g^2} \right) - \frac{2r_o^2}{r_t r_g} \cos\left[\frac{2\pi}{\lambda} (r_g - r_t) \right]}{2\left[1 - \cos\left(\frac{4\pi}{\lambda} \frac{h_s h_p}{w} \right) \right]} \right)^{\frac{1}{2}} \qquad (18)$$

where r_o = distance to probe from base of target
r_t = direct distance to probe from target segment
r_g = ground-reflected distance to probe from target segment
h_s = height of target segment
h_p = height of probe
$w = r \cos \psi$

The error in cross section is simply $-100 \times P^2$ percent, which indicates that measured cross sections for horizontal polarization are always low by this percentage. Assuming as before that $r_o = 60$ ft was used as the point for determining E_s^r (then extrapolated to $r = 100$ ft), the percentage error was plotted vs target height in Fig. 7 for angles of

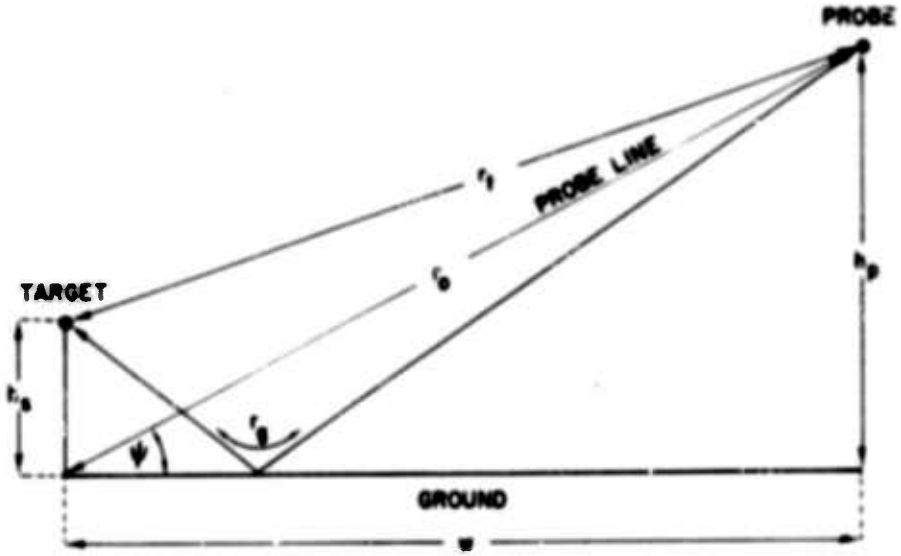

FIG. 6. RAY DIAGRAM FOR PHASE-ERROR ANALYSIS SHOWING TARGET AND PROBE POSITIONS RELATIVE TO THE GROUND AND EACH OTHER.

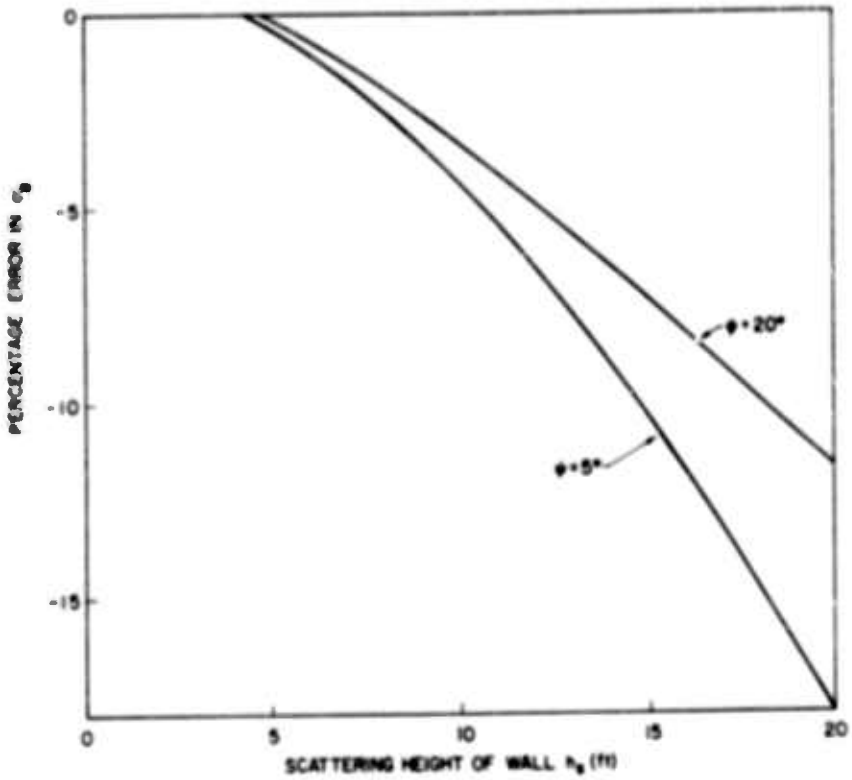

FIG. 7. MAXIMUM OBLIQUITY ERROR VS WALL HEIGHT FOR DIFFERENT ANGLES OF INCIDENCE.

incidence of 5° and 20°. Since the targets extended over all heights up to the maximum height for the wall, an "effective" height must be estimated. Since the actual incident radiation is greatest for the uppermost parts of the targets (for our target maximum heights), an estimate in cross-section error may be obtained from the figure. For target heights of 10 ft, the error is perhaps -2 percent; for 15-ft targets, -5 percent; and perhaps -8 percent for 20-ft targets.

A similar analysis for vertical polarization is difficult. However, it will be worthwhile to determine whether the error in cross section may be expected to be positive or negative at a particular angle of incidence. It must be pointed out that this error cannot necessarily be determined from the plots of E_s vs r. A positive error which decreases over a (perhaps small) range of r will cause an E_s range dependence faster than 1/r; likewise, a negative error which increases with range will cause the same effect. Whichever effect occurs, it is difficult to infer the error magnitude from the experimental plots, especially when cross sections are small (in light of other experimental errors).

Assume an "effective height" of the vertical target which scatters a direct ray and a ground-reflected ray to the probe. When the ground-reflected ray is above the Brewster angle, constructive interference will occur; likewise, destructive interference will occur below the Brewster angle; it was found that the Brewster angle is 14° for the terrain [Ref. 6, p. 20]. Finally, the probe and wall pattern gains will affect the magnitudes of the ground and direct rays. The discussion may be facilitated by considering two special cases: $\psi = 5°$ and $\psi = 20°$. Again, assume that $r_o = 60$ ft is used as the reference point for E_s extrapolation to far ranges (the errors will be the same for $r = 100$ ft). Assume an effective wall height of 10 ft.

At $\psi = 20°$, when the probe is located at r_o, the ground-reflected ray makes an angle of 28.4° with the ground; this angle decreases to 20° when the probe is far from the target. Since the path difference between the two rays from the target is always less than 1/4 wavelength, decreasing constructive interference will occur as one proceeds away from the target on the probe line. This causes a positive error. However, close to the target the probe and wall pattern gains tend to discriminate against

both rays. Since constructive interference occurs far out, a negative error is also introduced at $r_o = 60$ ft.

At $\psi = 5°$ the ground-reflected ray makes an angle of 14.3° with the ground; this decreases to 5° far out. At 5°, the reflection coefficient of the ground is near -1, and at 14° it is near zero. Far out, large destructive interference will occur, since the target is not very high (the path difference between rays is small); however, at r_o essentially only the direct ray exists. Hence a larger positive error exists at lower angles. Since for this case the ground-reflected ray is negligible at $r_o = 60$ ft, and since the angle that the direct ray makes with the probe is about the same far out, there are negligible errors caused by wall and probe gain patterns.

One may conclude that errors will be more positive for vertical polarization at lower angles of incidence as pointed out by Steele [Ref. 6, p. 17]. Moreover, these errors may be greater for lower wall heights, since greater destructive interference occurs for large r as a result of decreased path difference between ground and direct rays.

The transmitter was far enough from the target so that plane-wave illumination could be assumed [Ref. 12].

Target near-field effects were neglected.

Total errors in measuring a cross section are therefore about $[\pm(10 + 15/\sqrt{\sigma_B})-5]$ percent plus errors due to a phase-varying scattered field. Save for the latter, approximately the same errors may be expected for the measurement of free-space cross sections.

For $\sigma = 5\ m^2$, this gives a range of about +8 to -18 percent error plus phase change error. The phase error is about -5 percent for horizontal polarization, is positive (perhaps +100 percent or more) for very low angle vertical polarization, and is perhaps negligible for vertical polarization at 20° angle of incidence due to the balance of positive and negative errors. The cross-section results will be treated accordingly, in Chapter VII, by placing arrows on the appropriate data points to indicate the direction in which the measured cross sections should be moved.

V. ELECTRICAL CONSTANTS OF WALL

The dielectric constant and conductivity of the wall material were measured using a capacitor-Q technique. A drawing of the experiment is shown in Fig. 8. The capacitor was constructed from 3/32-in. aluminum

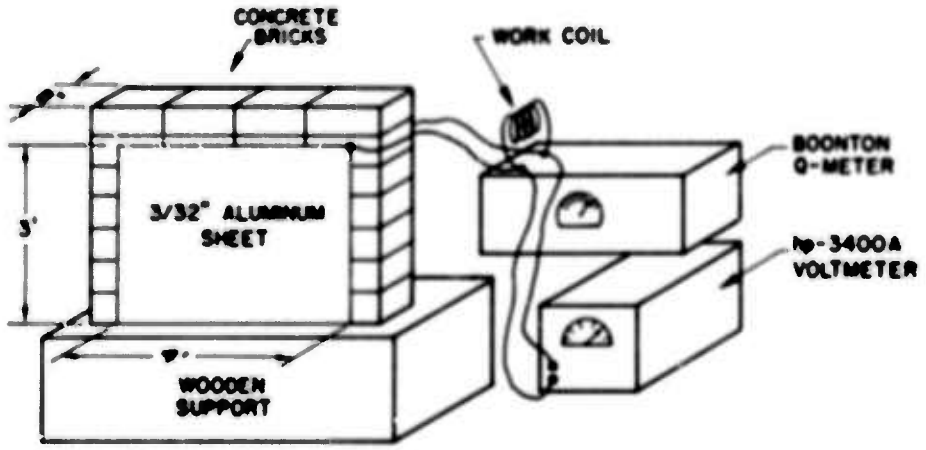

FIG. 8. DRAWING OF EXPERIMENT USING CAPACITOR-Q TECHNIQUE.

sheets and measured 3 ft by 4 ft. Two pieces of 8-in.-long heavy wire were connected to the corners of the sheets for measurement purposes. Values were measured for both wet and dry blocks, with and without vertical metal (supporting) rods inserted. The blocks were wetted by successive dunking in a clean water bath. The degree of total water permeation is expected to closely approximate that for the cases of backscatter measurement for the following reasons: (1) The blocks were exposed to the water for less time than for the wet walls measured (Fig. 3); however, water permeated the blocks' interiors as well; (2) drying of the blocks was slow, and therefore time was not an important factor. The metal rods were bundles of those used in construction of such walls and were spaced about 2.5 ft apart--much closer than in actual buildings. For all cases, the plates were covered with a watertight plastic jacket to eliminate leakage currents.

The procedure for obtaining the dielectric constants is set forth in the paragraphs below.

The capacitance of the plates was measured with a Boonton Q-meter at approximately 7 MHz, with and without blocks inserted; the circuit is

shown in Fig. 9. The dielectric constant is defined by $C = \epsilon_r C_o$, where C is the capacitance of the plates, ϵ_r is the relative dielectric constant of the material, and C_o is the free-space capacitance. Values obtained are shown in Table 2; $\epsilon_r = 2.0$ and 4.0 for dry and wet blocks, respectively, with or without metal rods. Note that the transfer function of the circuit [see Eq. (22)] gives

$$\frac{\partial T_2}{\partial C_T} = 0 \quad \text{at} \quad \omega = \omega_o = \frac{1}{\sqrt{LC_T}} \tag{19}$$

where C_T represents the total capacitance present in the circuit. Hence there are no errors present in determining the capacitance of the plates upon insertion of C and returning of the circuit (although R_s is nearly infinite when only C_{Qm}, the Q-meter C, is present). There is a small error due to the capacitance of the leads connected to the voltmeter; however, this was small enough to be neglected.

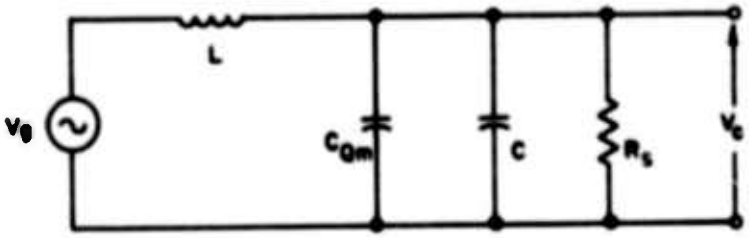

FIG. 9. CIRCUIT DIAGRAM OF CAPACITOR-Q TECHNIQUE.

TABLE 2. VALUES OBTAINED FOR CALCULATING ϵ_r USING THE CAPACITOR-Q TECHNIQUE

Wall Conditions	C_o (pf)	C_T (pf)	C_{Qm} (pf)	C (pf)	ϵ_r
Dry, no metal rods	116	332	99	233	2.0
Dry, with metal rods	116	332	98	234	2.0
Wet, no metal rods	116	496	30	466	4.0
Wet, with metal rods	116	488	30	458	4.0

The conductivity was measured as follows. The Q of the capacitor is related to the total resistance of the material by $Q = R_s \omega C$, where R_s is equivalently in parallel with C. Hence $R_s = Q/\omega C$ and $R_s = \frac{1}{\sigma}\frac{d}{A}$ where σ is the conductivity, d the thickness of the wall, and A the cross-sectional area. Hence

$$\sigma = \frac{0.182 \times \omega \times C}{Q} \quad \text{mho/meter} \tag{20}$$

where 0.182 takes into account the dimensions of the capacitor.

Referring to the circuit of Fig. 9, the voltage magnitude of the generator, V_g, was kept constant. The frequency of V_g was raised (or lowered) until the voltage V_c across the capacitor was $0.707 \times V_{co}$; $V_{co} = 1$ was the midband voltage value. This voltage was measured with an HP-3400A voltmeter which has 10-megohm input impedance, small input capacitance, short leads, and a bandwidth of 10 MHz. The upper and lower 3-db cutoff frequencies, f_u and f_ℓ, and the center frequency f_o were recorded. In this case $Q \neq f_o/\Delta f$. The circuit for which this applies is shown in Fig. 10.

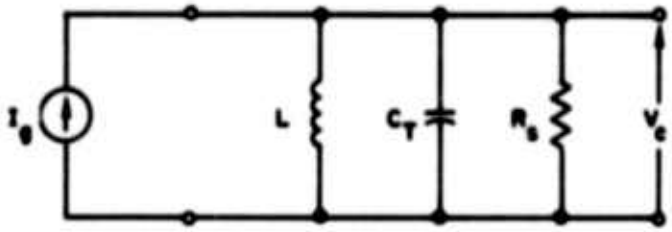

FIG. 10. CIRCUIT DIAGRAM FOR PROPER INTERPRETATION OF BANDWIDTH-Q RELATIONSHIPS.

The transfer function of this circuit is

$$\left|\frac{V_c}{I_g}\right|^2 = \frac{\omega^2 L^2}{(1 - \omega^2 LC_T) + (\omega^2 L^2/R_s^2)} = T_1 \tag{21}$$

However, the transfer function of our circuit is

$$\left|\frac{V_c}{V_g}\right|^2 = \frac{1}{(1 - \omega^2 LC_T)^2 + (\omega^2 L^2/R_s^2)} = T_2 \qquad (22)$$

A plot of relative magnitude vs relative fractional detuning is given in Ref. 13, p. 201. (This is a normalized plot termed the "universal resonance curve" and applies to the tranafer function $\sqrt{T_1}$.) Since $\sqrt{T_1} = \omega L\sqrt{T_2}$, we may adjust our relative voltage magnitudes of 0.707 at f_ℓ and f_u accordingly and thence obtain the quantity $a = Q_i[(f - f_o)/f_o]$ directly from the graph (where Q_i is the "indicated" Q of the circuit). Denote "actual" magnitudes by $V_{\ell o}$ and V_{uo} for $\sqrt{T_1}$, and by V_ℓ and V_u for $\sqrt{T_2}$. Then

$$V_{\ell o} = V_\ell \times \frac{f_\ell}{f_o} = 0.707 \times \frac{f_\ell}{f_o} \qquad \text{and} \qquad V_{uo} = 0.707 \times \frac{f_u}{f_o}$$

Reference to the plot gives a_u and a_ℓ at f_u and f_ℓ, respectively--thence giving Q_i. Owing to probable stray wiring capacitance and capacitor radiation, Q_i differed at the upper and lower points--the average was taken as a best approximation. Finally, since the Q-meter capacitance was also present in the circuit, we modify the Q_i's obtained by the ratio of plate to total capacitance, according to $Q_a = Q_i \times C/C_T$, where Q_a represents "actual" Q. The Q's for the capacitor were so low that there were no errors due to finite Q's of the work coil and Q-meter capacitor. Results for this experiment, together with the calculated σ's, are shown in Table 3.

With regard to the reflection coefficient of the wall, $\omega\epsilon$ is sufficiently larger than σ for both the wet and dry walls to enable neglect of the errors seen above due to the range in Q for upper and lower value frequencies. The method for obtaining ϵ_r is considered fairly accurate in light of aforementioned considerations.

The above-obtained values for σ and ϵ_r give

$$\epsilon_{rc_w} = \begin{cases} 2 - 10.916 \text{ dry wall} \\ \\ 4 - 11.74 \text{ wet wall} \end{cases} \qquad (23)$$

TABLE 3. VALUES OBTAINED FOR CALCULATING σ USING THE CAPACITOR-Q TECHNIQUE

Wall Conditions	f_ℓ (MHz)	f_o (MHz)	f_u (MHz)	a_ℓ	a_u	Average Q_i	Q_a	σ (mho/m)
Dry, no metal rods	5.91	6.30	6.59	-0.6	+0.43	9.52	6.68	$2.51(10)^{-4}$
Dry, with metal rods	5.91	6.30	6.59	Same	———	———	———	———
Wet, no metal rods	3.20	5.30	6.36	-1.10	+0.35	2.28	2.14	$1.32(10)^{-3}$
Wet, with metal rods	3.20	5.30	6.32	Same	———	———	———	———

After insertion of ϵ_{rc_w} in the formula for R_w, there results $R_{wd}(\frac{\pi}{2}) = 0.075$ (dry wall) and $R_{ww}(\frac{\pi}{2}) = 0.192$ (wet wall). Note that the metal supporting rods did not affect these values.

It must be noted that the blocks were not actually solid, but contained holes which constituted approximately one-half the wall volume. Although these holes are very much smaller than a wavelength, the reflection coefficient of the wall should be smaller than that for a solid wall. However, the capacitor measuring technique would also indicate decreased ϵ_r and σ. Therefore, it will be assumed that the reflection coefficient error is minimal as a result of the internal geometry of the blocks.

Finally, note that the electrical constants were measured at about 6 MHz, rather than 26 MHz. This was done to decrease capacitor radiation and it is therefore assumed that σ and ϵ_r are the same at both frequencies.

VI. FREE-SPACE RESULTS

Free-space cross sections were obtained in order to investigate the degree of applicability of physical optics theory to cross-section measurement. As mentioned previously, Steele and Barnum [Ref. 4] had first adapted the probe system to these measurements. Owing to close correspondence with microwave results, the method is considered accurate to within 10 to 20 percent (see Chapter IV). The wall sizes measured are shown in Table 4.

TABLE 4. FREE-SPACE RESULTS FOR VERTICAL POLARIZATION

Wall Size Height × Width	Wall Area (m^2)	B/I_L $(10)^{-3}$	σ_B Grounded (m^2)	σ_B Insulated (m^2)	R_w	σ_{Bo} (m^2)
10 × 10 Dry	9.27	2.035	7.84	3.47	0.075	0.045
10 × 10 Dry chicken wire	9.27	38.8	149.5	66.2	1.0 (0.328)	8.06 (0.862)
10 × 20 Dry	18.54	3.85	14.82	6.56	0.075	0.181
10 × 20 Wet	18.54	13.3	51.3	22.7	0.192	1.19
20 × 20 Dry	37.08	6.07	23.4	10.35	0.075	0.721

The experiment consisted of measuring the standing waves in front of a CW illuminated target at a very low angle of incidence. The transmitting antenna was placed on a 10-ft wooden mast, and the center of the probe was mounted on a self-supporting stand, 8 ft high, on which the telemetering antenna was fastened. The value of 1/V was recorded at 2.5-ft intervals, and these values were plotted vs w, as before [Ref. 4]. The method was not applicable for horizontal polarization since the vertical dimensions of the horizontal target were so large. Results were obtained for vertical polarization, however, as outlined below.

As before, an assumed background field was sketched in among the standing-wave perturbations. Values of E_s were then extracted from the plot by measuring the difference between the actual and the background field variations at the peaks and nulls. E_s was then plotted vs w, and a range dependence very similar to that exhibited by the "standard curve for vertical polarization" [Ref. 4] was found. From this, E_s (w = 30 ft) was found. By extrapolation of the background curve to w = 0, E_i was determined. Hence the quantity $B = |E_s^{30}/E_i|^2$ was calculated. On the same type of terrain, an "illumination factor," I_L, had been plotted vs target height for a transmitter-target separation of 300 ft [Ref. 4]. I_L as a function of target height takes into account the nonuniformity of target illumination caused by ground ray cancellation and hence was determined for each target height. From this, the "relative cross section" B/I_L was determined. B/I_L is related to the actual free-space cross section by a factor S defined by $\sigma = SB/I_L$. For well-grounded targets, $S = 1.705 \times 10^3$; for targets insulated from the ground, $S = 3.84 \times 10^3$. It should be noted that the S specification is valid since results obtained by Steele for a grounded quarter-wave monopole and a half-wave insulated dipole showed close correspondence at higher angles of incidence [Ref. 6, Fig. 6]--the minor deviations were due to increased obliquity effects for the half-wave target, and possible variations in vertical reradiation pattern with distance. Calculated results for both cases are shown in Table 4.

Since the wall was mounted in concrete only 2 ft deep, and since the conductivity of cement was found to be quite small, it is suggested that the wall was effectively insulated from the ground. Steele and Barnum [Ref. 4] measured the free-space cross section of an aluminum street lamp and an antenna mast; although these targets were mounted in concrete, they were also considered to be insulated. However, as was shown by Steele and Barnum for an aluminum mast, even when such a target barely touches the ground, the cross section changes (and hence so does S). This was termed the "poorly grounded case," and shows just how ambiguous the term "grounding" can be. We could, therefore, estimate the free-space cross sections as lying somewhere in between the two extreme cases calculated in Table 4.

This will not be done (even as it was not done for the street lamp and antenna mast, Ref. 4) in view of the results discussed below.

Wetzel has suggested [Ref. 7] that if $kh > 3$ (vertical polarization), where $k = 2\pi/\lambda$ and h is the height of the wall, we may apply geometrical optics to obtain the cross section at normal incidence. The formula is

$$\sigma_{Bo} = \frac{4\pi A_o^2}{\lambda^2} R_w^2(\tfrac{\pi}{2}) \qquad (24)$$

where A_o^2 is the physical area of the wall. σ_{Bo} was calculated for each size wall measured, and the results are also included in Table 4.

The ratio of $\sigma_B(\text{insulated})/\sigma_{Bo}$ is plotted vs the area of the wall in Fig. 11 on log-log scales. It was found that all the points fell on the curve drawn, except for the chicken-wire-covered wall. However, it was assumed that $R_w = 1$ for the chicken wire. If this value is changed to

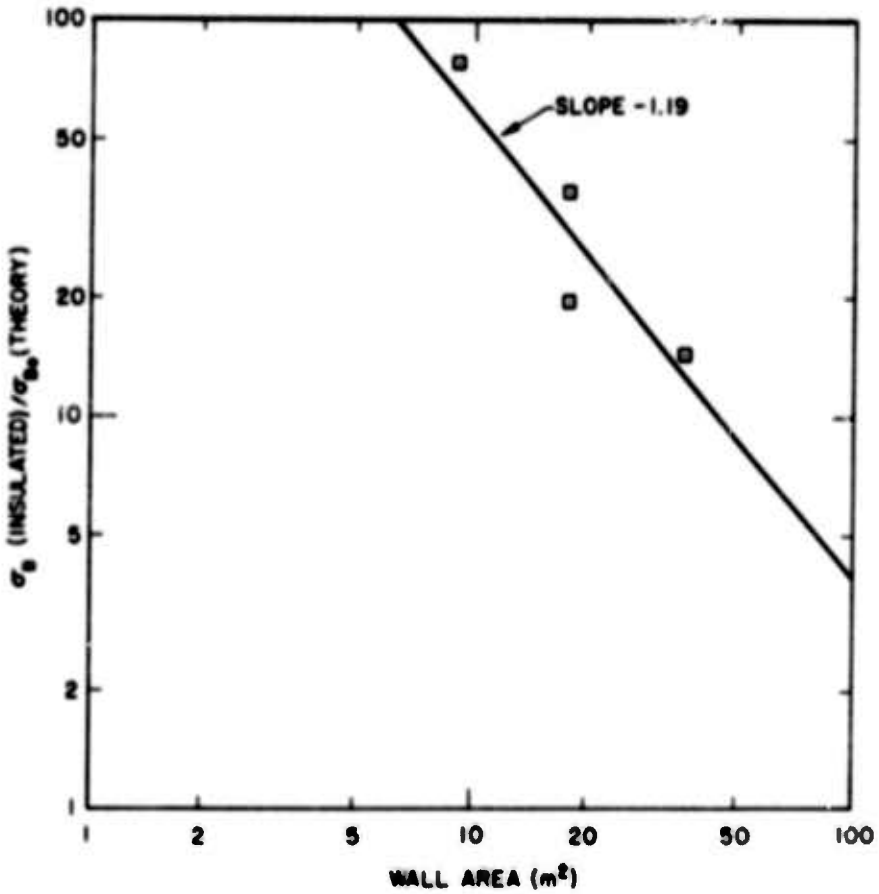

FIG. 11. PLOT OF $\sigma_B(\text{INSULATED})/\sigma_{Bo}(\text{THEORY})$ IN FREE SPACE VS AREA OF WALL.

$R_w = 0.328$ (which seems somewhat low), the point then falls near the 10- by 10-ft dry wall case, which it should (if the same theory is applicable). Note that it appears that cross sections are approximately proportional to wall area, rather than $(\text{area})^2$, for walls where $kh < 3$ (approximately).

It is encouraging to find that an asymptotic value near $\sigma_B/\sigma_{Bo} = 1$ is indicated for large walls. This indication will be strengthened in the next chapter when the (cross section)/(theory) ratio is plotted vs kh for both the free-space and angle-of-incidence measurements. Correspondence to theory is then indicated for $kh \approx 4$ or 5; it appears, therefore, that the Steele-Barnum technique is accurate to a good degree. Assuming that this is so, one should consider the walls to be insulated. If they were not, the plots vs kh would show that the correct asymptotic value of $\sigma_B/\sigma_{Bo} = 1$ would be indicated by walls (in free space) larger than those required to yield the same experiment-theory correspondence at different angles of incidence.

VII. RESULTS AT DIFFERENT ANGLES OF INCIDENCE

Cross sections at angles of incidence ranging between 2.5° to 22.5° were obtained for wall sizes ranging from 5 ft high and 10 ft wide, to 20 ft high and 20 ft wide. These results are plotted in Fig. 12a-j; Wetzel's theory (see Chapter II) is also plotted.

The results for vertical polarization are shown in Fig. 12a-h (the figures are listed in order of increasing wall area). Measured cross sections agree best with the theory for the larger walls and for angles of incidence between 10° and 20°; cross sections for smaller walls were well above the theory for all angles of incidence. This nonagreement is largely due to the inapplicability of the theory, and will be explored in a moment. Note first that a pronounced knee effect [Refs. 2,3,6] does not occur for most of the cases, even though it is predicted by the theory. However, one does note a tendency for decreased low-angle scatter for the larger walls. Actually, any apparent absence of the knee is probably due to experimental error, as discussed in Chapter IV. According to that analysis, one should drop the experimental points occurring below $\psi = 15°$ by perhaps 3 db or more. Also, as the wall area is made smaller, these points should be dropped more; it is difficult to determine the exact amount of the drop, but one might be guided by the shapes of the theoretical curves and place the experimental points on a line parallel to the theory. (For the larger walls, this practice is verified after noting similar experiment-theory curve shapes for horizontal polarization--e.g., Fig. 12j. However, as it is difficult to apply any theory to the smaller walls, one cannot adjust the data points strictly in the above fashion.) Note that points for $\psi = 20°$ should not be dropped, except perhaps 1 or 2 db for the 5- and 10-ft high walls; for these wall heights the positive errors will be greater, even for $\psi = 20°$. Moreover, negative errors caused by horizontal obliquity will be negligible for the 10-ft-wide walls, since the waves from the vertical wall edges are only about 4° out of phase with those from the center. In light of these required data adjustments, it is therefore very probable that the knee effect does occur, as predicted by the theory.

Figure 12b shows the cross sections for the 10- by 10-ft dry wall

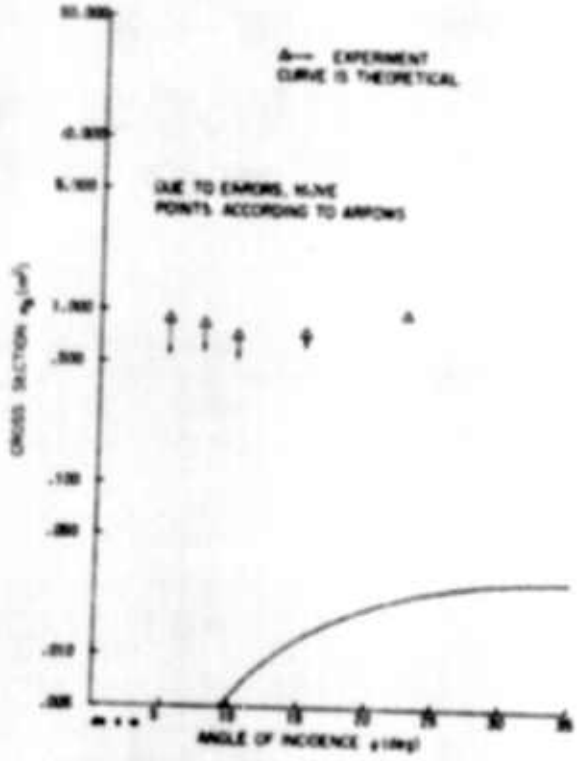

a. 5- by 10-ft dry wall; vertical polarization

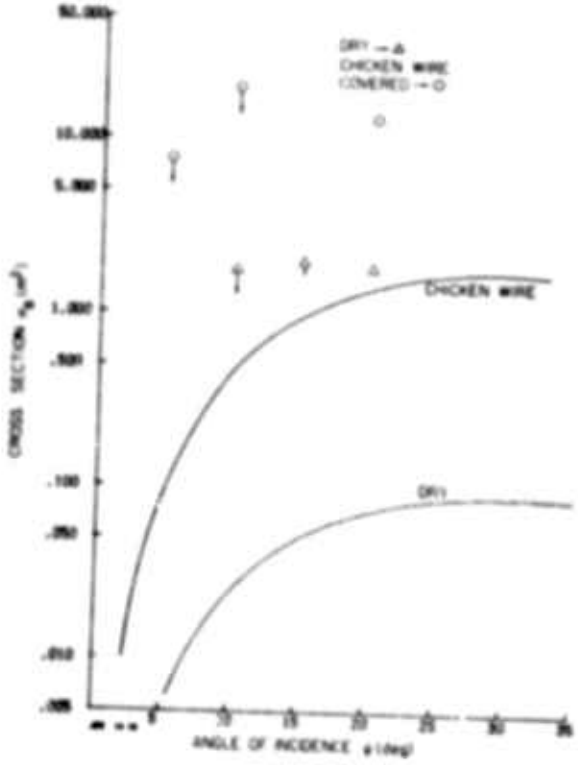

b. 10- by 10-ft dry and chicken-wire-covered wall; vertical polarization

c. 10
wi
pol

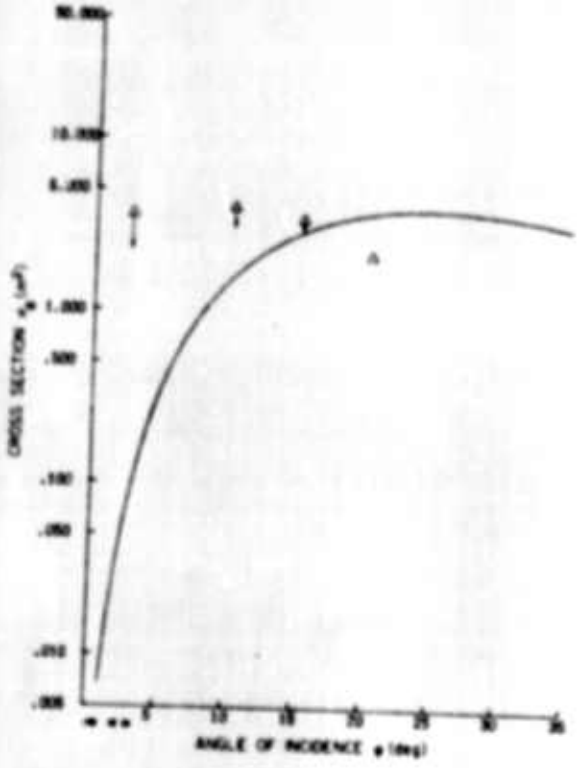

f. 15- by 20-ft wet wall; vertical polarization

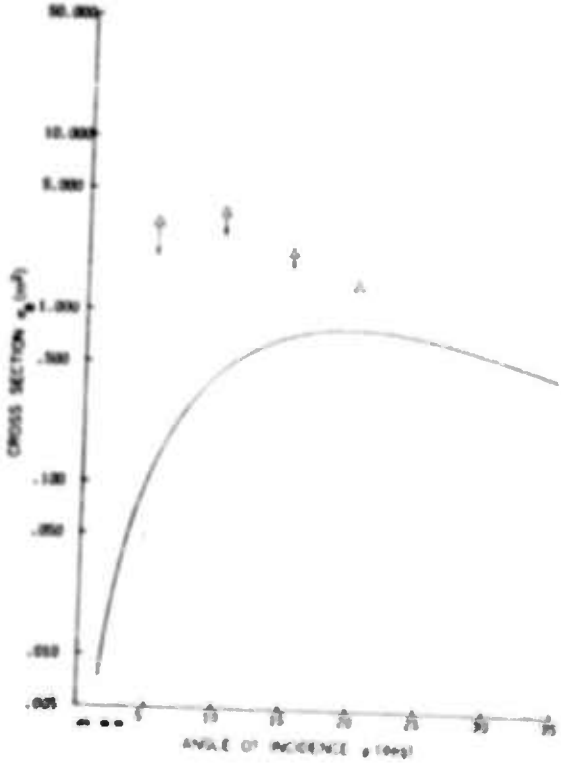

g. 20- by 20-ft dry wall; vertical polarization

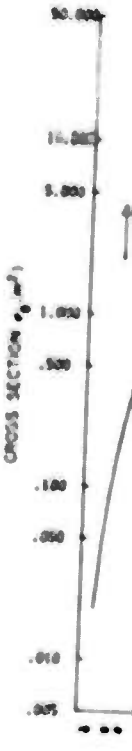

h. 20- b
polar

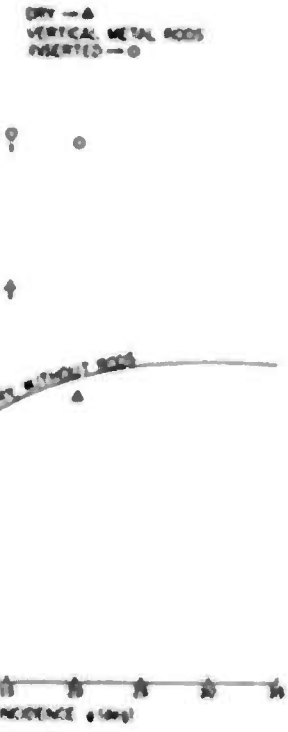

dry wall with and rods; vertical

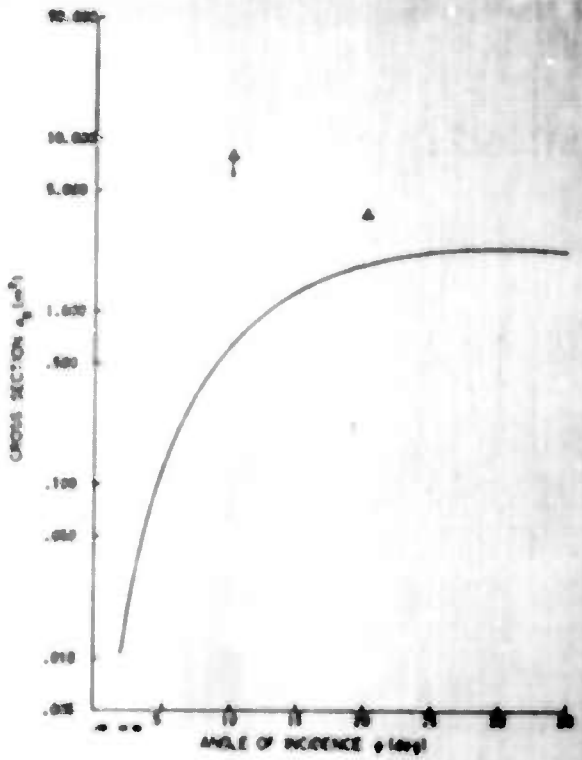

d. 10- by 20-ft wet wall; vertical polarization

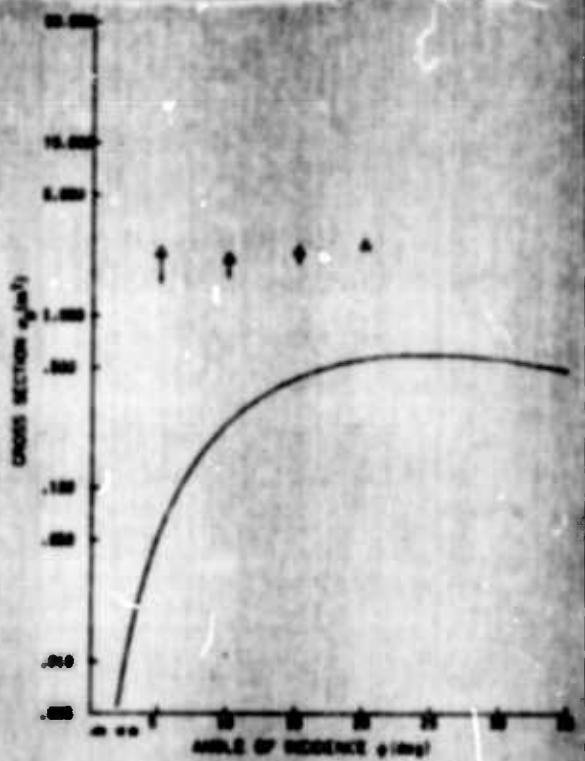

e. 15- by 20-ft dry wall; vertical polarization

vet wall; vertical

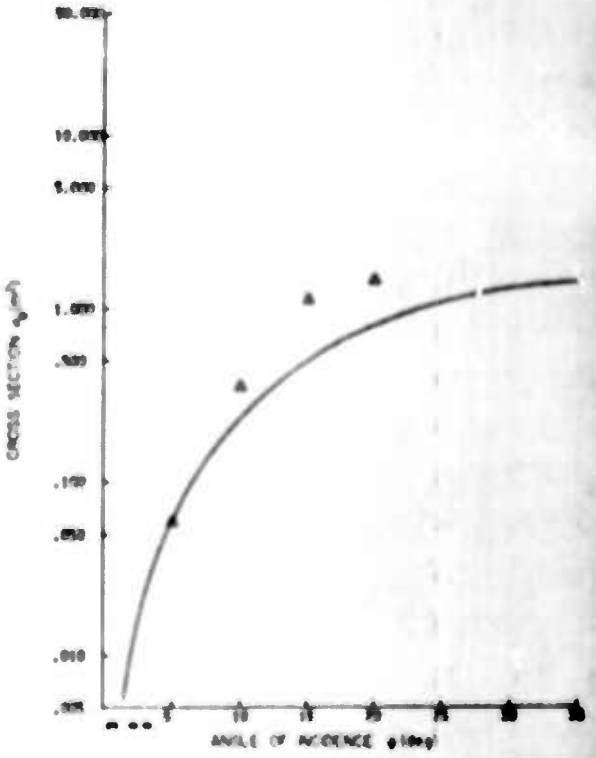

i. 20- by 20-ft dry wall; horizontal polarization

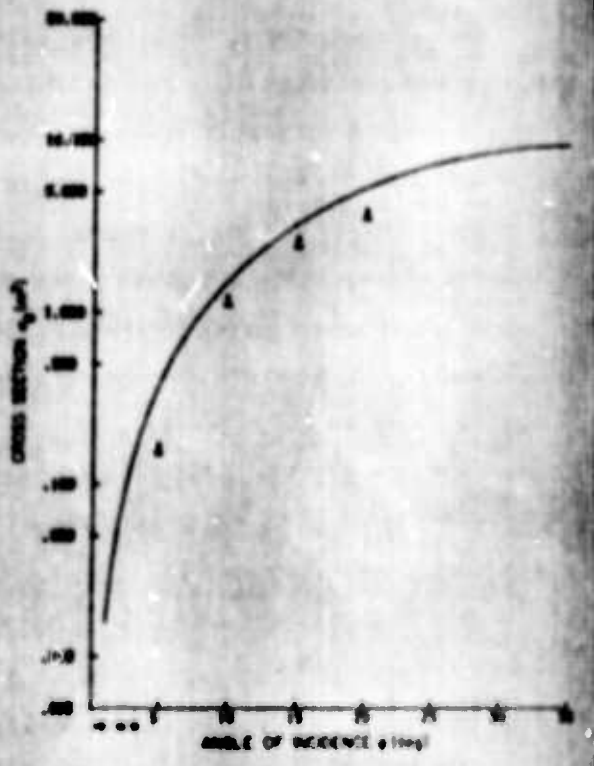

j. 20- by 20-ft wet wall; horizontal polarization

FIG. 12. CROSS SECTIONS VS ANGLE OF INCIDENCE FOR VARIOUS SIZES AND CONDITIONS OF WALLS COMPARED TO THEORY.

compared to the results for the same wall covered with chicken wire. The theoretical curve for the chicken-wire case assumes that $R_w = 0.328$, as derived in free-space measurement. As will be seen from the results for horizontal polarization, this value seems a little low; furthermore, cross sections deviate from theory for both cases by about the same amount. Therefore, it again seems probable that the R_{wd} (the dry wall's reflection coefficient) is also low. In any case, results at $\psi = 20°$ are most accurate, and at this angle the chicken wire increased the 10- by 10-ft dry wall's cross section by a factor of 7.32, or 8.65 db.

Figure 12c shows the cross sections for the 10-ft-high by 20-ft-wide dry wall compared to the results for the same wall with four vertical metal "supporting" rods inserted every 6.5 ft. The shapes of the curves are quite dissimilar since the cross sections for the dry wall were quite small, and experimental errors were therefore large (see Chapter IV). In light of these errors it will be more instructive to compare the two cases at $\psi = 10°$; the error caused by non-phase-constant E_s should be the same for the two cases. The horizontal obliquity error should be larger for the metal rod case, however, since the rods are the primary source of scatter, and 50 percent of the target is therefore concentrated at the horizontal extremities of the 20-ft-wide wall. Nevertheless, assume that the errors are identical, since the difference is probably not very large. The metal rods then give an increase in cross section of about 2.7, or 4.3 db, over the dry wall without the rods.

Only two curves (Fig. 12i-j) were obtained for horizontal polarization, since it was very difficult to detect any nonrandom perturbations in the background field for this polarization until the 20- by 20-ft wall size was reached (the 15- by 20-ft wall was not measured). Small cross sections were predicted by Steele [Refs. 6,11] and Wetzel [Ref. 7] for horizontal polarization; however, results for smaller walls, using vertical polarization, show that cross sections were much higher than predicted and it might be expected that the same would be true of horizontal polarization. To investigate this, curves for horizontal polarization (based on Wetzel's theory) are shown in Fig. 13. Comparison of these theoretical curves with those for vertical polarization for the smaller walls shows that cross sections for angles of incidence to 20° are considerably less than those

for vertical polarization until the larger walls are achieved. Steele [Ref. 6] found there same tendencies for a half-wave dipole, as shown in Table 5. This occurs since the major portion of illumination on the wall reached only its uppermost parts--as seen in the function of horizontal illumination factor, I_h [Ref. 4, p. 21]. In other words, horizontal cross sections increase very rapidly with increased vertical deviations of scatterers from zero height [Ref. 11]. Therefore, it is reasonable to predict that if actual cross sections deviate from the theory for smaller walls, the tendency will be the same ar for vertical polarization--as indicated in the results for the largest wall--after taking into account experimental errors (Chapter IV).

Figures 12i and 12j indicate that random errors in data reduction are relatively small, since the data points are parallel to smooth curves.

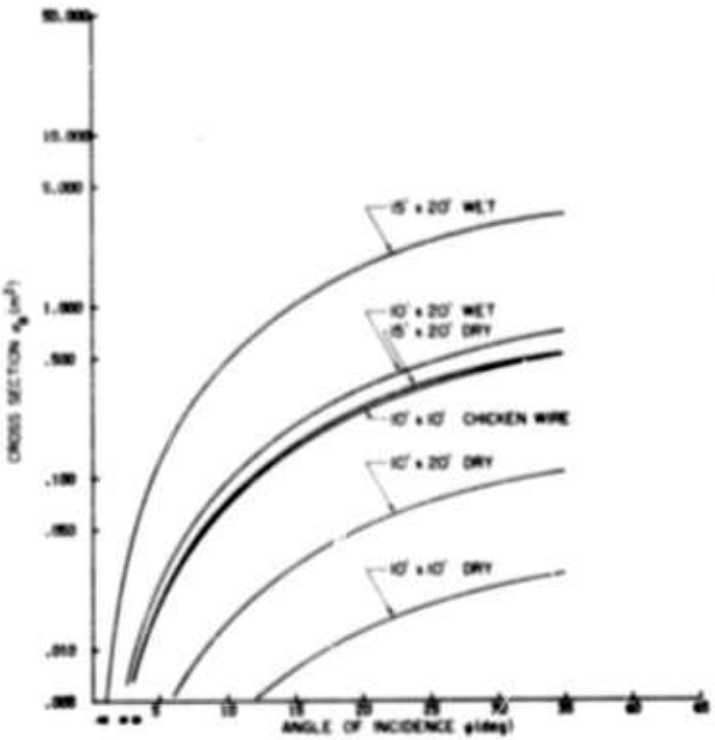

FIG. 13. THEORETICAL CROSS SECTIONS VS ANGLE OF INCIDENCE FOR SMALLER WALLS USING HORIZONTAL POLARIZATION.

Referring to Fig. 12j and after taking into account the negative errors occurring for horizontal polarization, the theory is closely realized for the 20- by 20-ft wet wall. However, there are larger deviations

TABLE 5. COMPARISON OF SCATTER FROM A HALF-WAVE DIPOLE AND A 20- BY 20-FT DRY WALL

Target	Free-Space Cross Section (m^2)	Cross Section at $\psi = 10°$	
		Horizontal Polarization (m^2)	Vertical Polarization (m^2)
$\lambda/2$ dipole	118	4 (h = 4 ft) 20 (h = 12 ft)	33
20- by 20-ft dry wall	10.35	0.35	3.75

from the theory for the 20- by 20-ft dry wall (Fig. 12i), especially for higher angles of incidence. Note that in Fig. 12f, cross sections for vertical polarization realize the theory quite closely for higher angles of incidence; furthermore, for these angles, it was seen that errors caused by a non-phase-constant scattered field were a minimum. Again, however, we note that when the same size wall was dry, cross sections were higher than theory for the same angles of incidence (Fig. 12e). Free-space results gave similar experimental deviations from the theory for the wall which was measured both wet and dry. Therefore it is suggested that either R_{ww} is too large or R_{wd} is too small. The latter seems more likely, since the conductivity of the wet material is higher and therefore the holes in the bricks probably do not affect the reflection coefficient of the wet walls as much.

It will be of interest to compare measured results to those predicted by theory, as was done for free-space cross sections. The angle ψ for which this comparison should be made must be chosen in light of all possible errors in both theory and experiment. Although phase errors in E_s are less at higher angles, so are most cross sections, and hence experimental errors are greater. The change in R_w with angle of incidence was neglected; this error will be greatest at higher angles of incidence. Also, ψ cannot be too small, since deviations from the correct curve shape are even greater at $\psi = 10°$. The comparison will therefore be made at $\psi = 15°$.

Figure 14a shows $\sigma_B(\text{experiment})/\sigma_B(\text{theory})$ vs kh plotted on log-log scales for $\psi = 15^\circ$ and for the free-space measurements; h is the wall height. There are four values of kh, corresponding to the four different wall heights. The points occurring for each of these four values were averaged and plotted in Fig. 14b. A straight line of best fit was drawn along these points and was transferred to Fig. 14a for comparison. The curve's slope is -2.55; if extrapolated, it would intersect the ordinate $\sigma_B(\text{experiment})/\sigma_B(\text{theory}) = 1$ at $kh \cong 5$. This curve may not be accurate near this point--indeed the line only represents a first-order estimation of low kh cross-section behavior.

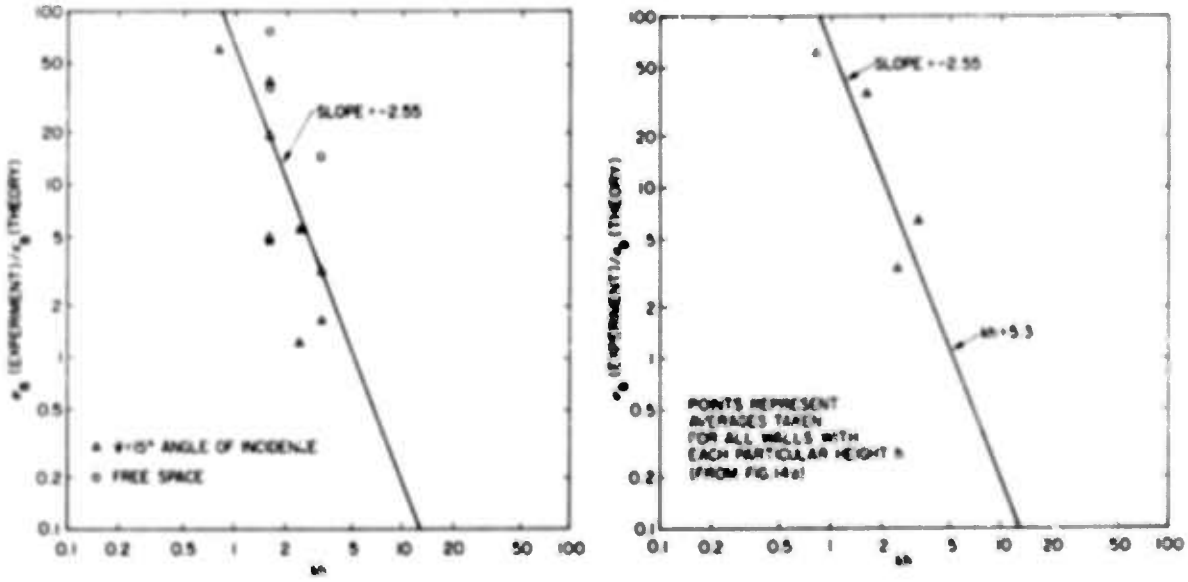

a. All points b. Points averaged

FIG. 14. GRAPH OF $\sigma_B(\text{EXPERIMENT})/\sigma_B(\text{THEORY})$ VS kh PLOTTED ON LOG-LOG SCALES. Points are for free space and $\psi = 15^\circ$.

Note (Fig. 14a) that the free-space points fall above the line and most of the 15° points fall below the line. Also note that if the wall were considered to be grounded, the free-space points would fall even further away from the line (higher)--therefore, the assumption (Chapter VI) that the wall is insulated from the ground is again justified.

It could be of future interest to plot the points from Fig. 14a vs the corresponding wall area, rather than kh, as was done in Fig. 11. Therefore, each of the values for $\sigma_B(\text{experiment})/\sigma_B(\text{theory})$ were plotted

vs the wall area. For each of the five wall areas, these values were averaged (as in Fig. 14b), and the average was also plotted vs the wall area (Fig. 15). Since the theoretical cross sections are proportional to $(\text{area})^2$, and a line of best fit among the points has a slope of -1.57, it is now suggested that actual cross sections may also be proportional to $(\text{area})^{\frac{1}{2}}$ for low kh. This is probably a more accurate estimate than that gained from Fig. 11, since more data points are involved in Fig. 15.

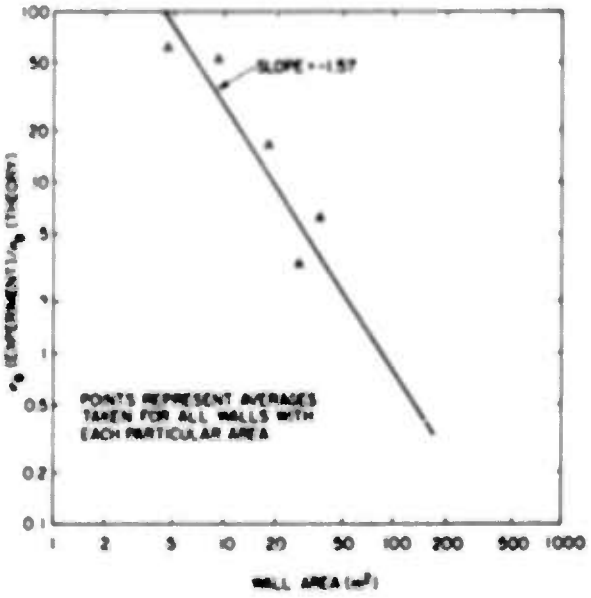

FIG. 15. GRAPH OF $\sigma_B(\text{EXPERIMENT})/\sigma_B(\text{THEORY})$ VS AREA OF WALL PLOTTED ON LOG-LOG SCALES FOR FREE SPACE AND $\psi = 15°$.

VIII. BACKSCATTER FROM BUILDINGS AND CITIES

In the following analysis vertical polarization will be assumed, unless otherwise indicated, since cross sections for the targets concerned were very much less for horizontal polarization. Furthermore, the angle of incidence ψ will be assumed to be 15° unless otherwise specified, since reference will be made to Fig. 14b. The frequency is assumed to be 25.9 MHz, although at times possible cross-section behavior may be considered at lower frequencies.

Figure 16 was taken from previous work done by Steele [Ref. 6, p. 26]. Cross sections obtained for the 20- by 20-ft wet wall (both polarizations) are also shown for comparison. It is interesting to note that for lower angles of incidence the cross sections for the wall were higher than those for the tree. Moreover, the knee effect for vertical polarization is not as pronounced for the wall. For angles of incidence between 10° and 15°, the vertical cross sections for the wall and tree were about the same.

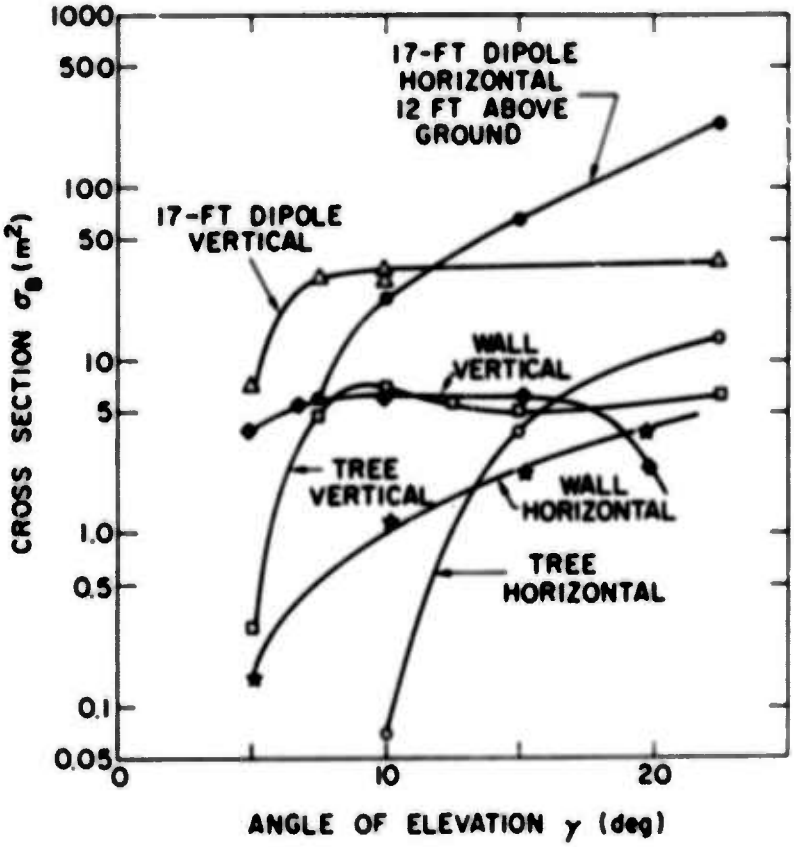

FIG. 16. CROSS SECTIONS FOR VARIOUS LAND TARGETS.

Comparison of the cross sections obtained for the 20- by 20-ft dry wall with those obtained by Steele for a large oak tree shows that the tree's cross sections were 1 to 2 db larger than the wall's.

Now, define an "average" wall to be 30 ft high and 60 ft wide. At 25.9 MHz, the theory was nearly applicable to the 20- by 20-ft wall, so one may estimate the cross section of the 30- by 60-ft wall to be 13 db higher.

Let us now construct a building with four such walls. Assuming that this building is randomly oriented, its cross section will be about 3 db less than the average wall's, for which the vertical plane of incidence was normal to the wall [Ref. 7].

It will be rather difficult to define the dimensions of an average building, since, as seen above, the theory does not apply for buildings with heights smaller than 1/2 wavelength or so; in fact, cross sections are then even higher than predicted. Moreover, Wetzel poin out that the decrease in a building's cross section due to random orientation is dependent upon its dimensions--the 3-db decrease applies to buildings with dimensions of the order of a wavelength; larger buildings will tend to produce more directive scatter, and hence will have smaller relative cross sections when randomly oriented. Let the average building be defined as above, with the understanding that most houses will be smaller, but that apartment complexes and most "downtown" structures tend to be as big or, usually, larger.

Next, consider the effects of structural supports and chicken-wire-covered structures such as plaster houses and buildings. It was found that vertical metal supporting rods added 4.3 db to a wall's cross section. The chicken wire added 8.65 db to the 10- by 10-ft wall's cross section. Since this was most likely caused by an increase in reflection coefficient, the same figure would apply to any size wall. Assume (conservatively) that a 5-db increase in a building's cross section occurs due to chicken-wire-covered structures and/or metal supports used in construction.

We have now arrived at the important (but somewhat approximate) result that a 60-ft-square by 30-ft-high, randomly oriented, dry cement (average) building will have a cross section at 25.9 MHz (-2 + 13 - 3 + 5) = 13 db higher than the large oak tree measured by Steele. Although most trees

are smaller than Steele's tree [Ref. 6], a tree's cross section increases roughly proportional to (height)^2 [Ref. 4], and forested areas usually contain a large proportion of trees larger than Steele's tree. Therefore, assume that the large oak tree measured by Steele represents an "average" tree. Hence, an average building has a cross section about 13 db larger than an average tree at 25.9 MHz. The results obtained by Steele and Barnum [Ref. 4, p. 46] show that the largest free-space cross section obtained for a tree was approximately 3 db larger than that for the tree measured by Steele; it is believed that the tree with the larger cross section was close to a resonant length and therefore represents one of the largest cross sections one would expect to measure for normal size trees. The average building has a cross section 10 db higher than this tree at 25.9 MHz.

Note that at lower frequencies the random orientation of buildings will cause a smaller decrease in a building's cross section, since the walls will produce less directive scatter. Moreover, tree cross sections should decrease very rapidly for lengths below 1/8 wavelength (or so) [Ref. 4, pp. 29, 31, 59]. Therefore, we may expect that buildings would produce significantly more scatter at lower frequencies, although it is difficult to infer from Fig. 14a that low-frequency (low kh) behavior is actually as approximated. Moreover, a dependence on building width was not deduced.

An attempt to generalize the above comparisons for a single tree and a single building to scatter from cities and forests could prove fatal, since the distribution of upright targets on an arbitrary terrain varies so widely; moreover, it has not yet been proven that land backscatter does indeed result from such upright targets. One can, however, make the following observations.

Since trees and street lights in cities are usually spaced much less than a wavelength from buildings and houses (effectively closer at lower frequencies), their effect may be likened to that caused by supporting structures in the buildings. One may therefore expect an additional increase in the cross section of a building that includes street lights since a street light was found to have a free-space cross section about 8 db larger than the "average" tree's [Ref. 4, p. 47].

Although horizontal scatter from trees and buildings is much smaller than that for vertical polarization, at low angles of incidence one may probably expect more horizontal scatter from cities as a result of power lines. This will be especially true at higher frequencies. For example, assume an average line height of 40 ft. The effectiveness of power and telephone lines will depend upon their height-from-ground/wavelength ratio. At particular heights, the path difference between direct and ground reflected rays is such as to cause total field cancellation at the line. Assuming that $R_g = -1$ for horizontal polarization, it may be seen from geometrical considerations that total cancellation occurs for

$$h_L = \frac{n\lambda}{2 \sin \psi} \qquad n = 0, 1, 2, \ldots$$

where h_L is the line height. Assume that 6.5 MHz is the frequency used; then $\lambda \approx 150$ ft and $\lambda/(2 \sin 15^\circ) = 289$ ft. Or, at $h_L = 145$ ft, complete constructive interference occurs. Since most lines are about 40 ft high, and both E_s and E_i are equally affected, the line's effective cross section compared to its maximum is given by

$$\left[\sin\left(\frac{40}{145} \times \frac{\pi}{2}\right)\right]^4 \times 100\% = 3.1\% \qquad (25)$$

This is quite small and results in probable negligible scatter from lines at this frequency, although many lines are several wavelengths long.

At 25.9 MHz, on the other hand, a similar analysis at $\psi = 15^\circ$ shows that scatter will be 95 percent effective from lines 40 ft high.

Since cross sections of lines are proportional to $(\text{length})^2$, one may expect significant horizontal scatter from cities at higher HF frequencies; however, the actual scattered power will, of course, also be a function of the line's gain pattern. See, for instance, Ref. 14.

Finally, note that rows of buildings are usually spaced in a fairly regular fashion--corresponding to a typical street map. One would therefore expect a backscatter signal enhancement at frequencies for which constructive interference occurs between reflections from adjacent rows. The "effective" row spacing is equal to $D[(\cos \psi)/(\sin \beta)]$, where D is the actual spacing, ψ is the angle of incidence, and β is the angle between

rays and rows. Constructive interference occurs for effective row spacings equal to multiples of 1/2 wavelength. The effect will not occur in forested areas since trees are usually positioned randomly. The signal enhancement effect would probably be noticed providing the city is very large or is surrounded by very small trees or open country.

Scatter from a large area containing many trees or buildings will be reduced by the "shadowing" of adjacent targets by their neighbors. Wetzel [Ref. 7] predicts that this effect will be greater for clusters of buildings.

Although an average building's cross section may be two orders of magnitude larger than that for an average tree, a particular illuminated area would probably contain many more (perhaps more than 100 times) trees than buildings. In light of this probability and the shadowing effect, it still appears that trees are, in general, the primary source of ground backscatter, if indeed such scatter results from upright ground targets. When there is prior knowledge of an illuminated target area, one might perhaps verify this prediction from records containing signal enhancements at particular frequencies. If signal enhancements are large for a particular study, it is very probable that city scatter is predominating.

IX. PROBE SYSTEM: MODIFICATIONS AND RECOMMENDATIONS

Since the probe system described by Steele and Barnum [Ref. 4] is rather unique, it is worthy of comment with regard to general applications. A block diagram of the system is repeated in Fig. 17; detailed design information has been given in Ref. 4.

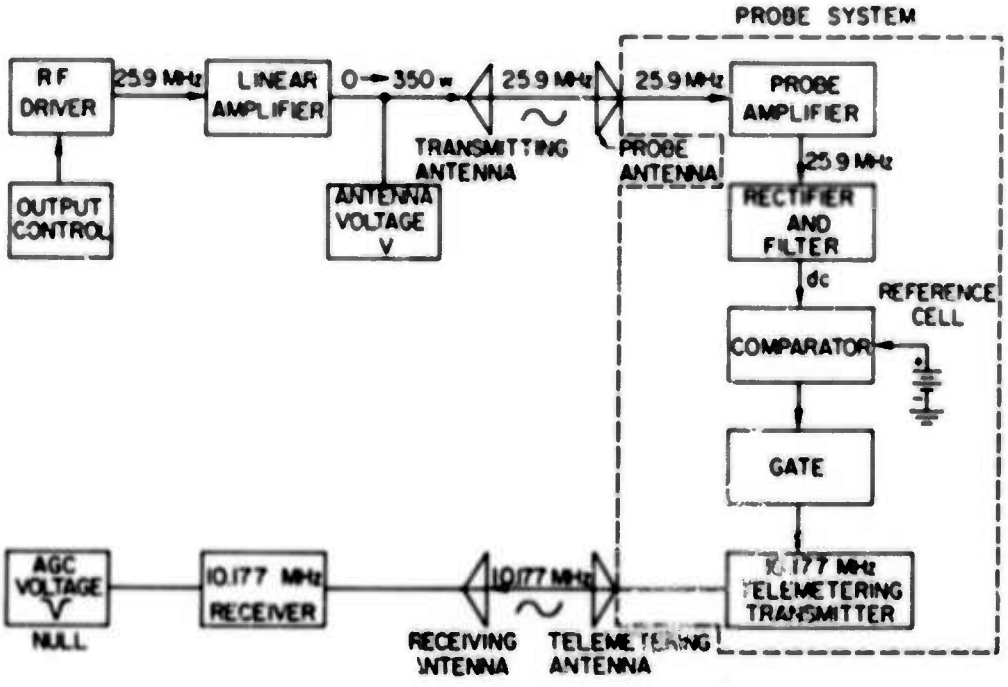

FIG. 17. BLOCK DIAGRAM OF PROBE SYSTEM.

Most important, Steele and Barnum were able to conclude that the probe was too small to upset the fields being measured, in the vicinity of CW illuminated targets. This fact referred to the probe's free-space radar cross section which is less than 0.1 m^2. It was not possible to measure this low a value, but it may be deduced through reference to cross sections obtained for cylinders in free space [Ref. 4, pp. 29, 31, 59]. Then, since

$$\sigma_B = 4\pi r^2 \left| \frac{E_s^r}{E_i} \right|^2 \tag{26}$$

we find that E_s (r = 10 m) < 1 percent of E_i (at the probe). Hence, if one were 10 meters away from a reflecting target, the resultant scattered

field would be less than 1 percent in error. This error will be less if the range dependence of the fields is faster than 1/r, which will be true in most instances near the ground. The error might be greater if the probe receives more illumination from the transmitter than the field point 10 meters away. At the probe's position, perhaps a 10-percent error exists. However, if the probe's polarization is maintained constant relative to the transmitting antenna, the error is also constant; it is therefore inconsequential since only relative field values are measured.

The telemetering antenna was found to introduce a slight constant attenuation to the fields being measured [Ref. 4]. An analysis similar to the above shows that its reradiation is negligible since its size was smaller than the probe.

For general applications, the telemetering antenna should be made smaller, through more efficient matching, and mounted perpendicular to the sensing antenna. Better still, since nonconstant field interference could still occur (with arbitrary probe orientations), a very high telemeter frequency could be chosen, and duplexing would then be possible. With this method, different probe orientations would not affect the attenuation caused by the close proximity of the probe sensing and telemetering antennas.

Since the probe system was constructed rather hurriedly, it was found later that other improvements could be made. A few comments regarding these improvements are in order.

A smaller probe sensing antenna would cause less field upset in the vicinity of the probe, but would also create less polarization discrimination. The latter effect could be decreased by reducing the size of the center box used for equipment housing. In general, construction practices and size limitation will be a function of the desired applications.

Further improvements can be made in the system gain magnitude and stability, telemeter null width and depth, transmitter output control, and telemeter AGC voltage monitoring.

System gain is primarily achieved in the probe amplifier. A first step would be to match the probe antenna to the amplifier input more efficiently. Increasing the gain of the probe amplifier without proper attention paid to amplifier stability would be disastrous. Also, care should be taken not to increase the amplifier noise figure, since noise will

contribute to output magnitude uncertainty, which in turn will decrease system accuracy due to AGC null broadening.

There are two primary causes of amplifier drift: (1) battery run-down, and (2) temperature changes caused by component joule heating and ambient temperature variations. The present scheme employs thermistor compensation to achieve temperature stability over a rather small temperature range; mercury batteries were used since they have the most constant output vs time characteristics. It was found that temperature variations were wide enough (on some days) to cause a monotonic gain drift--this is negligible if readings are taken over a short period of time, say 15 minutes. For longer measuring times, or if day-to-day comparisons are desired, some standard reference readings must be taken periodically which may be used to normalize sets of relative field readings. In other words, the null-producing probe field might change with time (temperature).

If more gain were achieved, or if wide temperature changes are anticipated, it appears that a negative feedback scheme would be most desirable, since a change in gain of 0.1 db is very noticeable. Therefore it would be useful to design a high gain amplifier, possibly using FET's as the active elements, employing low-frequency feedback, and preceded with a stagger-tuned, maximally flat narrowband filter tuned to the desired frequency. A bandwidth of 180 kHz (achieved with cascaded-signal-tuned circuits) proved adequate in the author's system. However, if adjacent channel interference is anticipated, or a particularly noisy target area is under study, a more narrow bandwidth would be necessary. The maximally flat filter would then be helpful in decreasing errors due to possible transmitter frequency and filter component drifts. As the gain is raised and more feedback used, more stable amplifier conditions result. However, the input impedance will also go down with more feedback--hence filter-matching problems will go up. A maximally flat notch filter in the feedback loop might then be helpful.

The telemeter could be first improved by increasing its RF output and by matching the telemetering antenna to the transmitter output (after perhaps decreasing antenna length). This would increase the effective range of the system and would place the null depth above the local noise level under more adverse conditions. With the present system (using a 4-ft telemetering antenna mounted 4 ft off the ground), a 1/4-mile range proved

to be about maximum. It was found empirically that as better matches were obtained between telemeter and telemeter antenna, the null depth lowered, thereby decreasing the null width and increasing the accuracy of the system. The surest way to increase the null depth is to better isolate the telemeter oscillator from the output amplifier which follows the gate. Furthermore, the gate should be designed to eliminate stray coupling and leakage currents--which occur between gate input and output wiring and across the gate diodes. Finally, means should be provided for obtaining a more balanced input to the gate.

Once the probe system accuracy is increased, it will be necessary to have a more vernicred transmitter output control; for decreased null width, the percent change required in transmitter output in order to achieve exact null will also decrease. Furthermore, a more sensitive meter, biased to the proper range, could be used for telemeter receiver AGC voltage monitoring. In fact, up to a certain point (which depends on the eyesight of the operator and the noise level) as this meter is made more sensitive, more "effective" null depth is achieved. Above all, a stable, narrowband telemeter receiver should be used.

General uses of the probe might include the measurement of antenna patterns, field leakages from transmitter buildings, underwater field distributions (after appropriate equipment housing is obtained), polarization discrimination, ground constants, or reflection coefficients. Note that these measurements can be made at only one frequency. If measurements at more than one frequency are desired, the frequency of the probe amplifier must be adjusted, and its antenna rematched. Care must then be taken not to approach the telemetering frequency too closely.

X. CONCLUSIONS

The results for cement brick wall cross sections, both as a function of wall size and angle of incidence (Figs. 11 through 13), and in free space as a function of wall size, indicate that corner reflector theory is closely approximated for larger walls at $kh \geq 5$. For these walls, a knee effect is clearly observed for vertical polarization but was not as pronounced as that for a large oak tree; this suggests that scatter from buildings may be higher than that from trees at the lower angles of incidence. For smaller walls, the knee was not observed but will still occur in light of experimental errors for lower angles of incidence. Backscatter was not measurable for horizontal polarization until the largest wall was reached; for each particular target, vertical cross sections were always higher than those for horizontal polarization.

Results for free-space cross sections show that for smaller walls cross sections may be proportional to area rather than to $(\text{area})^2$; later results at different angles of incidence suggested that these cross sections may actually be proportional to $(\text{area})^{1/2}$. For $0.8 < kh < 5.0$, cross sections also appear to be roughly proportional to $(\text{frequency})^{1/2}$, rather than $(\text{frequency})^2$.

A 30-ft-high by 60-ft-square, dry, randomly oriented building should have a cross section 13 db larger than a tree with a trunk 17 ft high and 4 ft wide, at 25.9 MHz.

Consideration of other city targets, primarily power lines, suggests that horizontally polarized scatter should be larger from cities than from forests, primarily at the upper end of the HF spectrum.

Since trees far outnumber buildings in large areas illuminated by HF radar, trees may be the primary source of vertically polarized ground backscatter. This prediction might be verified by noting that backscatter signal enhancements from cities should occur as a result of constructive interference between reflections from adjacent rows of buildings. For a particular backscatter record, the magnitude of these enhancements might provide an indication of a city's radar effectiveness, if targets on the illuminated land area were known.

Future work might include the measurement of cross sections of long lines at different angles of incidence and at different aspect angles. Other land targets, if isolated, could also provide useful information. It would be interesting to obtain, at a lower frequency as compared to 26 MHz, information regarding low kh cross-section behavior of walls and other targets.

REFERENCES

1. G. Hagn, "An Investigation of the Direct Backscatter of High-Frequency Radio Waves from Land, Sea Water, and Ice Surfaces," Final Report II, SRI Project No. 2909, Stanford Research Institute, Menlo Park, Calif., May 1962.

2. J. G. Steele, "Backscatter of Radio Waves from the Ground," Rept. SEL-65-064 (TR No. 109), Stanford Electronics Laboratories, Stanford, Calif., Jun 1965.

3. J. G. Steele, "Backscatter of 16 Mc/s Radio Waves from Land and Sea," Austral. J. Phys., 18, Aug 1965, pp. 317-327.

4. J. G. Steele and J. R. Barnum, "High-Frequency Measurement of Radar Cross Section Using the Standing-Wave Method," Rept. SEL-66-021 (TR No. 127), Stanford Electronics Laboratories, Stanford, Calif., Mar 1966.

5. R. W. P. King and T. T. Wu, The Scattering and Diffraction of Waves, Harvard University Press, Cambridge, Mass., 1959.

6. J. G. Steele, "High-Frequency Backscatter from Terrain with Trees," Rept. SEL-66-028 (TR. No. 128), Stanford Electronics Laboratories, Stanford, Calif., Apr 1966.

7. L. Wetzel, "On HF Ground Backscatter," unpublished paper, Institute for Defense Analyses, Arlington, Va., Oct 1965.

8. D. E. Kerr, Propagation of Short Radio Waves, McGraw-Hill Book Company, New York, 1951.

9. S. Ramo, J. R. Whinnery, and T. Van Duzer, Fields and Waves in Communication Electronics, John Wiley & Sons, Inc., New York, 1965.

10. F. E. Terman, Electronic and Radio Engineering, McGraw-Hill Book Company, New York, 1955.

11. J. G. Steele, "Influence of Electrical Properties of the Ground on the Backscatter Coefficient at High Frequency," Rept. SEL-65-110 (TR No. 121), Stanford Electronics Laboratories, Stanford, Calif., Dec 1965.

12. R. G. Kouyoumjian and L. Peters, Jr., "Range Requirements in Radar Cross Section Measurements," Proc. IEEE, 53, Aug 1965, pp. 920-928.

13. H. H. Skilling, Electrical Engineering Circuits, John Wiley & Sons, Inc., New York, 1963.

14. J. H. Van Vleck, F. Bloch, and M. Hamermesh, "Theory of Radar Reflection from Wires or Thin Metallic Strips," J. Appl. Phys., 18, 1947, pp. 274-294.

PAPERS TO BE PUBLISHED

1. J. G. Steele, "High Frequency Measurement of Radar Cross Sections Using the Standing Wave Method," in IEEE Trans. on Antennas and Propagation, July 1967.

2. J. G. Steele, "High Frequency Backscatter from Terrain with Trees," in Proc. IEEE.

3. J. R. Barnum, "High Frequency Measurement of Electric Fields Using a Telemetering Probe," in Electronics.

ONR-ARPA UNCLASSIFIED DISTRIBUTION LIST
March 1966

No. of Copies

NAVY

Chief of Naval Res.
Dept. of the Navy
Washington, D.C. 20360
1 Attn: Code 402
2 Attn: Code 418

Dir., Naval Res. Lab.
Washington, D.C. 20390
1 Attn: Code 5320
(Mr. J. M. Headrick)
1 Attn: Code 2027
1 Attn: Code 5320
(Mr. E. Zettle)
1 Attn: Code 5432C
(Mr. F. A. Polinghorn)

Chief of Naval Operations
Dept. of the Navy
Washington, D.C. 20301
1 Attn: OP-723E
1 Attn: OP-07TE

Dir., Special Projects Off.
Dept. of the Navy
Washington, D.C. 20360
1 Attn: Code SP-204

Commander
Naval Missile Center
Point Mugu, Calif. 93041
1 Attn: Code N03022

Commander
U.S. Naval Ord. Test Sta.
China Lake, Calif. 93557
1 Attn: Code 4025
(Mr. R. S. Hughes)

Commanding Officer and Dir.
U.S. Navy Elec. Lab.
San Diego, Calif. 92152
1 Attn: Mr. H. J. Wirth
1 Attn: Library
1 Attn: D. E. Chandler

No. of Copies

Commanding Officer
U.S. Naval Ord. Lab.
Corona, Calif. 91720
1 Attn: Mr. V. E. Hildebrand
(Code 453)

AIR FORCE

Foreign Tech. Div. (AFSC)
Wright-Patterson AFB, Ohio 45433
1 Attn: TDC (Mr. Zabatakas)
1 Attn: TDEED (Mr. W. L. Picklesimer)
1 Attn: TDATA (Mr. G. A. Long, Jr.)
1 Attn: TDCE (Mr. M. S. J. Graebner)

Headquarters, RTD
Bolling AFB
Washington, D.C. 20332
1 Attn: RTTC (Mr. Philip Sandler)

Rome Air Dev. Center
Res. and Tech. Div.
Griffiss AFB, New York 13442
1 Attn: EMASR (Mr. V. J. Coyne)
1 Attn: RAVEL-3 (Mr. G. R. Weatherup)
1 Attn: RALCS (Mr. Salvador DiGennaro)

Commander
USAF Security Service
San Antonio, Texas 78241
1 Attn: ORL (Mr. W. L. Anderson)

Headquarters, USAF
Off. of Assistant Chief of
Staff, Intelligence
Washington, D.C. 20330
1 Attn: AFNICAA (Lt. Col. Long)
1 Attn: Policy & Prog. Cp., AFNINC

Hqs., N. Amer. Air Def. Com.
Ent AFB
Colorado Springs, Colo. 80912
1 Attn: NPSD-A (Col. M. R. Cripe)
1 Attn: NELC-AP
1 Attn: ADOAC - ER
1 Attn: ADLPC-2A (Lt. Col. R. J.
Kaminski)

No. of Copies

Hqs., AFCRL
L. G. Hanscom Field
Bedford, Mass. 0173:
1 Attn: CRUP (Dr. G. J. Gassman)
1 Attn: CRUI (Mr. Stan Curley)

Hqs., USAF
The Pentagon
Washington, D.C. 20301
1 Attn: AFRDDF (Lt. Col. Eugene A. Novak)

Hqs., SAC
Offutt AFB
Omaha, Nebraska 68113
1 Attn: Mr. Eugene Jackson

ESD (ESSL)
L. G. Hanscom Field
Bedford, Mass. 01731
1 Attn: Col. R. J. Kuehn (440L)

ARMY

Chief, Army Security Agcy.
Arlington Hall Station
Arlington, Va. 22212
1 Attn: ATOP-O (Mr. W. Mulroney)
1 Attn: Mr. R. R. Neill

Commanding Officer
U.S. Army Security Agency
Processing Center
Vint Hill Farms Station
Warrenton, Virginia 22186
1 Attn: Technical Library
1 Attn: Lt. Han Bagully

Commanding General
U.S. Army Material Command
Washington, D.C. 20313
1 Attn: AMCRD-D (Dr. C. M. Hudson)

U.S. Army Elec. Labs.
Mt. View Office
P.O. Box 205
Mt. View, Calif. 94042
1 Attn: Mr. Joseph Bert

No. of Copies

U.S. Army, SLAG
1B-657, The Pentagon
Washington, D.C. 20505
P.O. Box 715
1 Attn: Mr. N. R. Garofalo

U.S. Army Foreign Service and Tech. Center
Munitions Bldg.
Washington, D.C. 20315
1 Attn: Communications and Electronics Div.

Office of Assistant Chief of Staff for Intelligence
Dept. of the Army
Rm. 2B457, The Pentagon
Washington, D.C. 20301
1 Attn: Mr. Joseph Grady

DOD

Dir., Adv. Res. Proj. Agcy.
Washington, D.C. 20301
1 Attn: Mr. Alvin Van Every

Director
Weapons Sys. Evaluation Group
Off. of the Dir. of Def. Res. and Eng.
1 Washington, D.C. 20301

Office of the Assistant Dir.
Intelligence and Reconnaissance
Office of the Dir. of Def. Res. and Eng.
Rm. 3E119, The Pentagon
Washington, D.C. 20301
1 Attn: Mr. Howard A. Staderman

Director, Def. Intelligence Agcy.
Room 3B259, The Pentagon
Washington, D.C. 20301
1 Attn: AQ-2A2 (Capt. Michael Hudock)
DIAST-2B (Lt.Col. P. N. Keriakou)
DIAAQ-2A
1 Attn: DIAQ-2 (Maj. Julian Godwin)

No. of Copies

Deputy Dir., Res. and Tech.
Office of the Dir. of Def.
Res. and Eng.
Rm. 3E1030, The Pentagon
Washington, D.C. 20301
1 Attn: Dr. Chalmers W. Sherwin

Office of the Assistant Dir.
(Defense Systems)
Def. Res. and Eng.
Rm. 3D138, The Pentagon
Washington, D.C. 20301
1 Attn: Mr. Daniel Fink

Dir., National Security Agcy.
Ft. George G. Meade, Md. 20755
1 Attn: K-344 (Mr. Charles Candy)
1 Attn: C3/TDL

Def. Doc. Center
Cameron Station
20 Alexandria, Va. 22314

National Aero. and Space Admn.
Ames Research Center
Moffett Field, Calif. 94035
1 Attn: Dr. Kwok-Long Chan
1 Attn: Mr. Lawrence Colin

OTHER

ITT Electrophysics Labs, Inc.
3355-52nd Ave.
Hyattsville, Md. 20781
1 Attn: Mr. William T. Whelan

Astrophysics Res. Corp.
10889 Wilshire Blvd.
Los Angeles, Calif. 90024
1 Attn: Dr. Alfred Reifman

HRB Singer, Inc.
Science Park
State College, Pa. 16801
1 Attn: Library

Institute for Def. Analyses
400 Army-Navy Drive
Arlington, Va. 22202
1 Attn: Dr. Paul Von Handel

No. of Copies

Institute of Science and Tech.
The Univ. of Michigan
P.O. Box 618
Ann Arbor, Michigan 48105
1 Attn: BAMIRAC Library

Mass. Inst. of Tech.
Center for Space Res.
Bldg. 33-109
Cambridge, Mass. 02138
1 Attn: Dr. J. V. Harrington

Mass. Inst. of Tech.
Lincoln Lab.
Lexington, Mass. 02173
1 Attn: Dr. J. H. Chisholm

MITRE Corp. - E Bldg.
Rm. 353
Bedford, Mass. 01730
1 Attn: Mr. W. A. Whitcraft, Jr.

National Bureau of Standards
Boulder Labs.
Boulder, Colorado 80301
1 Attn: 85.20 (Mr. L. H. Tveten)

Pickard and Burns, Inc.
Res. Dept.
103 Fourth Ave.
Waltham, Mass. 02154
1 Attn: Dr. John C. Williams

Princeton Univ.
James Forrestal Res. Center
Sayre Hall
Princeton, N.J. 08540
1 Attn: Dr. Edward Frieman

Electronics Res. Lab.
Univ. of Calif.
Berkeley, Calif. 94720
1 Attn: Prof. D. J. Angelakos

RAND Corp.
1700 Main St.
Santa Monica, Calif. 90406
1 Attn: Dr. Cullen Crain
1 Attn: Library

No. of Copies

Raytheon Company
Communication and Data
Processing Operations
1415 Boston-Providence Turnpike
Norwood, Mass. 02062
1 Attn: Mr. L. C. Edwards

Stanford Res. Inst.
Menlo Park, Calif. 94025
1 Attn: Dr. David Johnson

Sylvania Electronic Systems
Applied Research Lab
40 Sylvan Rd.
Waltham, Mass. 02154
1 Attn: Library

Mr. Thurston B. Soisson
Box 8164 SW Station
1 Washington, D.C.

Sylvania Elec. Systems
Electronic Def. Labs.
P.O. Box 205
Mt. View, Calif. 94042
1 Attn: Mr. John DonCarlos

University of California
Mathematics Dept.
Berkeley, Calif. 94720
1 Attn: Dr. Edmond J. Pinney

Battelle-Defender
Battelle Memorial Inst.
505 King Ave.
Columbus, Ohio 43201
1 Attn: Doc. Center

Dept. of Elec. Eng.
Radiolocation Res. Lab.
University of Illinois
Urbana, Illinois 61803
1 Attn: 311 EERL (Mr. D. G.
Detert)

No. of Copies

Bendix Corp.
Bendix Radio Div.
Baltimore, Md. 21204
1 Attn: Mr. John Martin

The Univ. of Texas
Elec. Eng. Res. Lab.
Rt. 4, Box 189
Austin, Texas 78756
1 Attn: Mr. C. W. Tolbert

Rice University
Fondren Library
P.O. Box 1892
1 Houston, Tex. 77001

Purdue University
Library
1 Lafayette, Ind. 47907

DOCUMENT CONTROL DATA - R & D

(Security classification of title, body of abstract and indexing annotation must be entered when the overall report is classified)

1. ORIGINATING ACTIVITY (Corporate author)
Stanford Electronics Laboratories
Stanford, California

2a. REPORT SECURITY CLASSIFICATION
UNCLASSIFIED

2b. GROUP

3. REPORT TITLE
HIGH-FREQUENCY BACKSCATTER FROM TERRAIN WITH BUILDINGS

4. DESCRIPTIVE NOTES (Type of report and inclusive dates)
Technical Report

5. AUTHOR(S) (First name, middle initial, last name)
J. R. Barnum

6. REPORT DATE
January 1967

7a. TOTAL NO. OF PAGES
50

7b. NO. OF REFS
14

8a. CONTRACT OR GRANT NO
Nonr 225(64), NR 088 018;

8b. PROJECT NO
ARPA Order 1966-67

8c.

8d.

9a. ORIGINATOR'S REPORT NUMBER(S)
TR-130

9b. OTHER REPORT NO(S) (Any other numbers that may be assigned this report)
SEL-67-002

10. DISTRIBUTION STATEMENT
Each transmittal of this document outside the agencies of the U.S. Government must have prior approval of the Office of Naval Research, Field Projects Branch, Washington, D.C. 20360.

11. SUPPLEMENTARY NOTES

12. SPONSORING MILITARY ACTIVITY
Office of Naval Research

13. ABSTRACT

It is becoming more apparent that a fair proportion of high-frequency backscatter from level portions of the earth's surface results from upright targets such as trees and buildings. Using the standing-wave method, at 26 MHz, trees have been investigated at angles of incidence (with respect to the horizontal) up to 22.5°. It was found that a tree may provide significant scatter.

The present undertaking was to measure--by the same technique--backscatter from cement walls of different sizes and conditions at 26 MHz. Using a balloon-borne transmitting antenna and telemetering probe, cross sections for both horizontal and vertical polarization were obtained for angles of incidence between 2.5° and 22.5°. Magnitudes of cross sections were much greater for vertical polarization at lower angles of incidence.

For angles of incidence other than broadside, but with the radiation perpendicular to the intersection of the wall and the ground, the wall-ground combination behaved as a corner reflector; the experimental results for larger walls showed agreement with the corresponding theory. Subsequent extrapolation of the theory suggests that buildings may have cross sections much higher than trees.

A comparison of wall scatter to that from a large oak tree, and consideration of other city targets, suggests that at low angles of incidence horizontally polarized scatter should be larger from cities than from forests, primarily at the upper end of the HF spectrum. Although an average building may have a cross section as much as 16 db larger than that for an average tree, trees far outnumber buildings in the large areas illuminated by HF radar; therefore, trees may be the primary source of

DD FORM 1 NOV 65 1473

14 KEY WORDS	LINK A		LINK B		LINK C	
	ROLE	WT	ROLE	WT	ROLE	WT
HIGH-FREQUENCY RADAR HIGH-FREQUENCY BACKSCATTER LAND RADAR TARGETS						

ABSTRACT (Cont)

vertically polarized ground backscatter. A knee was observed in the curves for cross section vs angle of incidence; however, the knee was not as pronounced for the wall as that occurring for a large oak tree. This variance suggests that scatter from buildings may be higher than that from trees at the lower angles of incidence.

Backscatter signal enhancements from cities at particular frequencies might provide an indication of the magnitude of building scatter from a particular target area.